Moment tensor inversion of Explosive Long Period events recorded on Arenal Volcano, Costa Rica, constrained by synthetic tests

R. Davi, G.S. O'Brien, I. Lokmer, C.J. Bean, Philippe Lesage, M. Mora

Moment tensor inversion of Explosive Long Period events recorded on Arenal Volcano, Costa Rica, constrained by synthetic tests.

R. Davi[1], G.S. O'Brien[1, 2], I. Lokmer[1, 2], C.J. Bean[1, 2], P. Lesage[3], M.M. Mora.[4]

[1]Seismology and Computational Rock Physics Laboratory, School of Geological Sciences, University College Dublin, Belfield, Dublin 4, Ireland.

[2]Complex and Adaptive Systems Laboratory (CASL), University College Dublin, Belfield, Dublin 4, Ireland.

[3]Laboratoire de Géophysique Interne et Tectonophysique, CNRS, Université de Savoie, 73376 Le Bourget-du-Lac Cedex, France

[4]Escuela Centroamericana de Geología, Universidad de Costa Rica, Ciudad Universitaria Rodrigo Facio, San Pedro de Montes de Oca, 214-2060 San José, Costa Rica.

Abstract

In order to constrain the moment tensor solution of an explosive seismic event recorded on Arenal volcano, Costa Rica, we perform tests using synthetic data. These data are generated using a 3D model including the topography of the volcano and the best estimation of the velocity model available for Arenal. Solutions for (i) the moment tensor components, and (ii) the moment tensor plus single forces, are analysed. When noisy data and mislocated sources are used in the inversion, spurious single forces are easily generated in the solution for the moment tensor components plus single forces. Forces also appear when the inversion is performed using an explosive event recorded on Arenal

in 2005. Synthetic tests indicate that these forces might be spurious. However the mechanism is correctly retrieved by the inversion in both solutions. The ability to recover the explosive mechanism for the 2005 event combined with the interpretative aids from the synthetics tests will enable us to invert for the large variation in events observed on Arenal.

Keywords: Arenal volcano, moment tensor inversion, single forces, synthetic tests

1. Introduction

Volcanoes are complex and challenging environments showing a great variety of behaviour. A range of earthquake types are regularly recorded on volcanoes. They include: high frequency tectonic-like events, also known as volcano tectonic events, (VT), explosions, long period events (LP) and tremor. VT events have energy in the range of 2-20 Hz with very similar signatures to tectonic earthquakes. They are due to brittle rock failure, generated by regional tectonic forces, dyke propagation or pore over-pressure (McNutt, 2005). LP events and tremor are normally characterized by strongly peaked spectra. Their energy is concentrated between 0.2 and 5 Hz and they are thought to be caused by fluid movements inside volcanic conduits (Chouet, 2003). Since tremor and LP events seem to have common characteristics, differing only in duration, some authors believe they share the same source mechanism (Chouet, 1996; Neuberg et al., 2000). These types of events often precede and accompany volcanic eruptions, hence a deeper knowledge of their source origin may be helpful in volcanic event forecasting.

One of the most common tools used to retrieve the seismic source mechanism is a moment tensor inversion. The combination of moment tensor components represents a system of equivalent forces that produces the same wavefield as the actual physical processes at the source. Inverting for the seismic source mechanism has become a common procedure. Inversions for very long period events (VLP) have been successfully performed (Ohminato et al., 1998; Chouet et al., 2003) as the very long wavelengths are not influenced by structural heterogeneities. However, this is not always the case for inversions of LP events. The shortest wavelengths are sensitive to velocity structures and strong topographic effects (Bean et al., 2008; Lokmer et al., 2007; Lokmer et al., 2008; Métaxian et al., 2009). Such effects introduce many uncertainties in the inversion procedure that can lead to apparently stable, but erroneous solutions (Bean et al., 2008). In fact, due to the complexity of volcanic environments (e.g. the lack of sufficient structural information, the high degree of heterogeneity and the scattering effects due to the pronounced topography), it is quite difficult to recover a unique (and correct) source mechanism. The inclusion of single forces in the inversion procedure makes the recovery of the source mechanism an even more challenging task. However, single forces may be common in volcanic environments and have been modelled in other seismic source studies. Takei and Kumazawa (1994) provide a theoretical justification for the physical existence of these forces. However, an accurate quantification of these forces is not available at present. This is due to the fact that an inversion procedure with an increased numbers of free parameters is extremely sensitive to uncertainties in the near-surface velocity model (Bean et al., 2008).

In this paper, we perform a moment tensor inversion of an explosive event recorded in 2005 on Arenal volcano, Costa Rica, using constraints obtained by synthetic tests. Topographical and structural effects are reduced using the best estimation of velocity model available for Arenal volcano and Green's functions are calculated including 15 m resolution digital elevation model of the volcano. In the synthetic tests we assess our ability to retrieve the correct source time function and mechanism when (i) random noise is added to the data, and (ii) the source location is not accurately known. We also investigate how the presence of single forces affects the moment tensor solution. We aim to quantify our ability to accurately recover the true source from real seismic data. The information obtained by performing the synthetic tests is used in the analysis and interpretation of the solution of the inversion performed on real explosion data from Arenal. The methodology used in the calculation of the Green's functions, and in the inversion method, is provided herein. Results of our synthetic tests, the inversion of the real event and the interpretation of the mechanism that generates this event are also presented.

2. Arenal volcano

Arenal is a small strato-volcano located in north-western Costa Rica and is mainly composed of tephra and lava flows (Soto and Alvarado, 2006); its location and digital elevation model are shown in Figure 1. It was dormant for several centuries until July 1968 when a Peléan eruption resulted in 78 fatalities and opened three new craters in the western flank. Arenal's explosive activity is still ongoing today and is preceded, and

accompanied, by different types of seismic events. The most common types are LP events, explosions, spasmodic and harmonic tremor, rockfalls and sporadic volcano tectonic swarms (Alvarado and Barquero, 1997). Explosions and LP events have the same frequency range (1-3 Hz), but differ in amplitude. Explosions have larger amplitudes and are accompanied by a large, audible air-shock. The explosion coda often evolves into tremor (Hagerty et al., 2000). Tremor is the most common type of event at Arenal with a duration that can last for several hours and comprises spasmodic and harmonic. Harmonic tremor can be distinguished from spasmodic tremor by their regularly spaced frequency peaks with most of the energy concentrated between 0.9 and 2 Hz. Spasmodic tremor energy spans 1-6 Hz. There is no clear difference in the genesis of spasmodic and harmonic tremor; the former can progressively evolve into the latter and vice-versa (Lesage et al., 2006). Most of the tremor exhibits a progressive gliding in frequency that can last tens to hundreds of seconds. The gliding phenomenon can be generated by pressure changes in the fluid inside the conduit (Hagerty et al., 2000). The number of seismic events can be variable during the day. However, in recent decades a decrease in the number and amplitude of explosions has been recognised (Lesage et al., 2006). Arenal's seismicity is often accompanied by gas emissions produced during the explosions and by passive degassing in rhythmic pulses along the edge of the crater (William–Jones et al., 2001). The origin of these seismic events is, at present, not fully understood.

3. Methodology

The elastic Green's functions are defined as the Earth's response to an impulsive source generated at a certain point (source location) and propagating to a receiver location in an elastic Earth. The n^{th}-component of the displacement, recorded at position $\mathbf{x}$ and time t, can be written as (Aki and Richards, 2002):

$$u_n(\mathbf{x}, t) = M_{pq}(t) * G_{np,q}(\mathbf{x}, t) + F_p(t) * G_{np}(\mathbf{x}, t), \qquad \text{n, p, q = 1, 2, 3} \qquad (1)$$

where M_{pq} is the force couple or dipole in the pq direction acting at the source, F_p is the single force acting in the p direction, and G_{np} and $G_{np,q}$ represent the n^{th} components of the corresponding medium responses (Green's functions) and their derivatives, respectively. The asterisk indicates convolution and the summation convention applies. Volcanoes are the most "promising" environments in which single forces are likely to be found (Takei and Kumazawa, 1994), even if the existence of these single forces in the LP process is, at present, not reliably constrained by experiments or observations. For VLP events, Chouet (2003) attributes single forces to gravitational energy in the source volume due to the ascent of a slug of gas in the volcanic conduit or by a volcanic jet during an explosion. The latter phenomenon was also successfully modelled using single forces in the recent work of Jolly et al. (2010). The reliability of the inversion results are strongly dependent on the accuracy with which the Green's functions are calculated (Lokmer, 2008). In the past, due to computational restrictions, Green's functions were calculated only for a homogeneous half-space excluding topography. This approach leads to misinterpretations because the seismic wavefield is sensitive to layered velocity models and strongly affected by topographical scattering (Bean et al., 2008). However, in

140 the past decade, topography has been included in the calculation of Green's functions
141 (Ohimanto and Chouet, 2007; Neuber and Pointer, 2000; Jousset et al., 2004; Jolly et al,
142 2010). To avoid incorrect interpretations we require detailed information about the
143 medium i.e. a precise velocity model or near-accurate Green's functions relative to the
144 frequencies of interest. At present, detailed velocity models with structural information,
145 particularly related to the layers close to the surface, are extremely rare on volcanoes due
146 to the considerable cost and effort involved in producing such high resolution velocity
147 models. Therefore, synthetic tests provide a powerful tool for constraining the inversion
148 results and improving the reliability of such interpretations.
149
150 To calculate the Green's functions we use 3D-full wavefield numerical simulations
151 including topography and the "best" estimate of the velocity structure retrieved from
152 sounding using the spatial autocorrelation (SPAC) method, Métaxian et al., 1997, and
153 seismic refraction experiments carried out on Arenal in 1997 (Mora et al., 2006). In this
154 study, we use the 3D Elastic Lattice Method (ELM), to simulate wave propagation in the
155 elastic medium (O'Brien and Bean, 2004). To calculate the Green's functions we use a 1-
156 D velocity model (Figure 2). This velocity model comprises two major layers following
157 the profile of the topography above a half space medium with velocities of 3.5 km/s for
158 the P-waves (V_p) and 2.0 km/s for the S-waves (V_s) and a maximum density equal to
159 2500 kg/m^3. The numerical domain consists of a 13 x 11 x 6 km^3 space where topography
160 is derived from the Digital Elevation Model (DEM) of the volcano using a spatial grid
161 step of 15 m. Long wavelengths are simulated using a model of large extent with
162 relatively small grid-step. Absorbing boundaries, 900 m thick, are included in the model

to avoid edge reflections and ensure the absorption of the longest wavelengths. The top boundary of the model is a free surface including topography. To calculate the Green's functions library for a large number of source locations within a predefined source region, we adopt the Reciprocity Theorem (e.g. Aki and Richards, 2002). Green's functions are calculated over a volume (480 x 300 x 840 m^3) of 4735 points located under the crater summit. In addition to calculating the Green's functions for each single point source, we also required their spatial derivatives around the source position. Spatial derivatives can be extracted directly from the output of the simulation and are given by the central finite-difference derivative

$$G_{np,q}(\mathbf{r},\mathbf{s}) \approx \frac{G_{np}(\mathbf{r},\mathbf{s}+\Delta q) - G_{np}(\mathbf{r},\mathbf{s}-\Delta q)}{2\Delta q} \qquad (2)$$

where $G_{np,q}(\mathbf{r},\mathbf{s})$ is the spatial derivative of the Green's functions G_{np} around the source position, $\mathbf{s}$ is the source position, $\mathbf{r}$ is the receiver position and Δq is the spatial grid spacing. The Green's functions were calculated using a Gaussian source time function with a frequency range of up to 5 Hz and a duration of 15 s. The recording positions for the synthetic data map to the real locations of nine stations deployed on the volcano during a seismic experiment carried out in February 2005, as shown in Figure 1. Since Arenal is quite a dangerous environment (due to the frequent pyroclastic flows and the ballistic bombardment of blocks and bombs), the stations were deployed on the flanks of the volcano but, unfortunately, could not be placed close to the summit.

In the frequency domain, equation (1) can be written as:

186

187 $$u_n(\mathbf{x}, \omega) = M_{pq}(\omega) G_{np,q}(\mathbf{x}, \omega) + G_{np}(\mathbf{x}, \omega) F_p(\omega) \quad (3)$$

188

189 where $u_n(\omega)$, $M_{pq}(\omega)$, $F_p(\omega)$, $G_{np}(\omega)$, $G_{np,q}(\omega)$, are the spectra of the displacements, of

190 the moment tensor components, of the single forces and of the components and of the

191 spatial derivatives of the Green's functions, respectively. The equation is solved

192 separately for each frequency. The results are then transformed into the time domain

193 using an inverse Fourier Transform. Equation (3) can be written in matrix form as:

194

195 $$\mathbf{u} = \mathbf{Gm} \quad (4)$$

196

197 where **u** is the data matrix, **G** is matrix containing the Green's functions and derivatives,

198 **m** is the moment tensor and single forces components' matrix. If N is the number of

199 seismograms used in the inversion, equation 4 can be also written in an explicit form as;

200

201 $$\begin{bmatrix} u_1 \\ u_2 \\ \cdot \\ \cdot \\ \cdot \\ u_N \end{bmatrix} = \begin{bmatrix} g_{11,1} & g_{12,2} & g_{13,3} & g_{11,2} & g_{11,3} & g_{12,3} & g_{11} & g_{12} & g_{13} \\ g_{21,1} & g_{22,2} & g_{23,3} & g_{21,2} & g_{21,3} & g_{22,3} & g_{21} & g_{22} & g_{23} \\ g_{31,1} & g_{32,2} & g_{33,3} & g_{31,2} & g_{31,3} & g_{32,3} & g_{31} & g_{32} & g_{33} \\ \vdots & \vdots & \vdots & \vdots & \vdots & \vdots & \vdots & \vdots & \vdots \\ \vdots & \vdots & \vdots & \vdots & \vdots & \vdots & \vdots & \vdots & \vdots \\ g_{N1,1} & g_{N2,2} & g_{N3,3} & g_{N1,2} & g_{N1,3} & g_{N2,3} & g_{N1} & g_{N2} & g_{N3} \end{bmatrix} \cdot \begin{bmatrix} M_{11} \\ M_{22} \\ M_{33} \\ M_{12} \\ M_{13} \\ M_{23} \\ F_1 \\ F_2 \\ F_3 \end{bmatrix} \quad (5)$$

202

203 with the assumption (due to the symmetry of the moment tensor) that

$$g_{np,q} = \begin{cases} G_{np,q} & p = q \\ G_{np,q} + G_{nq,p} & p \neq q \end{cases} \qquad n = 1,2,3,..N \tag{6}$$

The quality of our inversion procedure is tested through the evaluation of the misfit (R) between calculated and observed data. R can be expressed by the following equation:

$$R = \frac{(\mathbf{u} - \mathbf{Gm})^T \mathbf{W} (\mathbf{u} - \mathbf{Gm})}{\mathbf{u}^T \mathbf{W} \mathbf{u}} \tag{7}$$

where $\mathbf{W}$ is a diagonal weighting matrix of the quality of the waveforms. It can be expressed in explicit matrix format as

$$W = \begin{bmatrix} w_1 & 0 & \cdots & 0 \\ 0 & w_2 & \cdots & 0 \\ \vdots & \vdots & \ddots & \vdots \\ 0 & 0 & \cdots & w_N \end{bmatrix} \tag{8}$$

The lowest value of the misfit R indicates the best solution for $\boldsymbol{m}$. As equation 4 is a linear equation, its least squares solution can be expressed as (Menke, 1984):

$$\mathbf{m}^{est} = \left(\mathbf{G}^T \mathbf{W} \mathbf{G}\right)^{-1} \mathbf{G}^T \mathbf{W} \mathbf{u} \tag{9}$$

where the superscript "T" denotes the transpose matrix and $\mathbf{m}^{est}$ is the estimated moment-tensor matrix. Since data recorded at different stations can show different noise signatures, the weight matrix plays an important role in the inversion procedure.

4. Description and results of Synthetic Tests

The inversion technique is normally very sensitive to a range of effects present in volcanic environments such as those associated with topography, near surface structures and heterogeneities. To test the consistency and limitations of our inversion procedure we performed a series of synthetic tests. In these tests we attempt to (i) investigate our ability to retrieve the correct source time function and mechanism for a fixed source location when random noise is added to our synthetic data, and (ii) analyze how a mislocated source position can influence the inversion solution while highlighting the role played by the single forces.

The use of synthetic tests is of crucial importance to contribute to the understanding of the inversion technique and to retrieve the correct mechanism acting on the volcano. Using 3D numerical simulations we generate synthetic signals with a Ricker wavelet source time function with a central frequency of 2 Hz, shown in Figure 3. The source is positioned under the crater summit where the real source is most likely to be located (Benoit and McNutt, 1997; Hagerty et al., 2000; Mora et al., 2001; Lesage et al., 2006). Source locations are not fully constrained at depth but the epicenters are probably located in a small area centered under the active crater (Métaxian et al., 2002). We fix our source

point at a depth of 200 meters beneath the crater summit. The mechanism simulated is an explosion ($M = 10^{12}$ Nm). No single forces are included. The inversion was performed for both a moment tensor plus single forces (MT+SF), and moment tensor only (MT).

It is important to note that in the following tests the moment tensor parts of the source solution are expressed in 10^{12} Nm, while the force parts are expressed in 10^{9} N. This is due to the fact that a force of 10^{9} N will produce a displacement with the same amplitude of a moment of 10^{12} Nm if their radiation patterns are ignored (radiation pattern can be ignored because of the good azimuthal coverage of the deployment). We validate (not shown here) that this holds for our station configuration, i.e. that the radiation patterns of the obtained moments and forces do not introduce significant deviation from the general rule outlined above. Consequently, if we plot moment and forces using the same scale, forces will not be visible in the diagrams even if they contribute considerably to the total amplitude of the signals.

The first test aims to show the ability of our inversion code to retrieve the exact mechanism and source time function. Since we used the exact Green's functions calculated for the exact source position, the correct solution is expected to be retrieved. Figure 4 shows the results of the test for the moment tensor components plus single forces (MT+SF) in the left panel and moment tensor only (MT) in the right panel using the field location of the nine stations. Solutions are characterized by a small value of the misfit (approximately equal to zero). Since the source time function and the mechanism are perfectly recovered by the inversion, and the value of R is small, we can affirm that

the correct solution is retrieved by our inversion code for both solutions (MT and MT+SF). Table 1 lists the values of the misfits of the inversions performed using synthetic and real data.

Since data recorded on volcanoes can often have a low signal-to-noise ratio, we attempt to simulate a real situation by adding noise to our synthetic data. In the frequency range of interest, we contaminate our synthetic dataset with random noise derived from the noise level of the real data recorded on Arenal. These data show a low level of contamination of noise equally distributed at all the stations. The amplitude of the noise is within 10% of the average rms amplitude (signal-to-noise ratio, SNR = 10). The inversion is performed for the moment tensor components and the moment tensor components plus single forces. Results of the test are illustrated in Figure 5. Spurious single forces appear in the MT+SF inversion solution. Since the amplitude of the noise is small, the solution is not dominated by the spurious forces and the source time function and explosive mechanism are correctly recovered by both inversions (see M_{xx}, M_{yy}, M_{zz} components for MT and MT+SF solution). In order to test how larger noise amplitudes influence the solution we increased the noise level to 50% of the average rms amplitude, which could be the case if strong tremor was recorded simultaneously with LP events. The amplitude of the spurious forces increases with the increase in noise level. As shown in Figure 6 (right panel) the MT solution remains stable and correct, while in the case of MT+SF the spurious single forces strongly contaminate the solution. The source time function and mechanism recovered along the diagonal components of the moment tensor solution (MT+SF) are no longer correctly retrieved and the solutions do not look stable.

291 This leads to the conclusion that noise introduces a larger error into the inversion with
292 more free parameters.
293
294 Since spurious single forces can be generated when noisy data are used in the inversion,
295 we want to investigate how the presence of real single forces can influence the solution.
296 In order to understand the role played by single forces in the inversion procedure for both
297 MT and MT+SF solution, we perform synthetic tests in which different geometries are
298 simulated (e.g. pure volumetric source and a vertical crack with the normal parallel to the
299 x direction) along with including a strong single force in the west-east (x) direction.
300 Again twelve stations have been used along with a signal to noise ratio of 10. Results for
301 the pure volumetric source ($M = 10^{12}$ Nm) and single force ($F = 10^{9}$ N) are shown in
302 Figure 7. Solutions for the moment tensor components (Figure 7, right panel) are
303 correctly retrieved by the inversion procedure even though a real single force is included
304 in the actual input source. In the solution for the MT+SF (Figure 7, left panel), spurious
305 single forces are generated in the vertical and north-south directions, in addition to larger
306 amplitudes along the z direction. The amplitude of the west-east force is successfully
307 retrieved, while the source-time function exhibits “ringing” in the tail of the retrieved
308 signal. Results for a vertical crack with single west-east horizontal force are shown in
309 Figure 8. The MT inversion solution (Figure 8, right panel) is well resolved, but spurious
310 single forces are again generated for the MT+SF solution, left panel of Figure 8. For the
311 vertical crack the spurious force along the z direction has a slightly larger amplitude than
312 the one generated for a pure volumetric source. For both geometries along the off-
313 diagonal components, a small non-volumetric component is generated. The generation of

this component can be considered as an artifact of the inversion procedure and it does not significantly affect the solution.

The same test has been performed using an input single force along the vertical direction. The MT solutions are correct for pure volumetric sources and vertical crack geometries. In the solution for MT+SF, the moment tensor part and the vertical force are again correctly retrieved while spurious single forces are present in the north-south and west-east directions. Since the same solutions have been obtained using a west-east and a vertical input force, only solutions for the horizontal force is presented.

Finally a test is performed to analyze how the solution of the moment tensor inversion for MT and MT+SF is influenced when an incorrect source position is used. The signal to noise ratio is again 10. With this test we aim to resemble a realistic, and quite common, situation in which the correct position of the seismic source is unknown and difficult to determine. The mislocated source is fixed in a positioned 240 m in the x-direction, 345 m in the y-direction and 500 m in the z-direction away from the correct source (located under the crater summit at a depth of 200 m). In the test, an explosive source mechanism has been simulated with no single forces included in the inversion. The solution is shown in Figure 9. For the MT solution the explosive mechanism and the Ricker-like wavelet source time function are well retrieved by the inversion. In the MT+SF solution spurious single forces are generated, particularly in the z-direction. The amplitudes of the spurious single forces originating from a mislocated source position are comparable to the amplitudes of the forces generated when noise is added to our synthetic data (see Figure 5

and 9). This leads to the conclusion that in the presence of a noise with amplitude within 10% of the average rms, the solution is insensitive to the inaccurate location of the source.

5. Discussion of synthetic tests

We performed the synthetic tests in order to constrain the inversion of the real data from Arenal volcano. In particular, we wanted to investigate how different signal to noise ratios, and errors in the source locations, influence the inversion solutions. We also tested the inversion code using synthetic data generated with 3D numerical simulations. We have shown that results for noisy data give stable MT solutions in which the source time function and mechanism are correctly retrieved. In the case where forces are allowed in the solutions (MT+SF), spurious single forces are generated with the largest amplitudes in the z-direction. When the signal to noise ratio decreases, the amplitude of the spurious single forces increases, strongly influencing the solution. When the signal to noise ratio is decreased to 2, the source time function and mechanism are no longer retrieved in the MT+SF solution. In addition, the spurious single forces entirely dominate the solution. Finally, we tested the sensitivity of the inversion to source mislocation. In this case the correct source time function and mechanism are correctly retrieved for the MT solution, while solutions for the MT+SF give rise to spurious single forces. Since both the source mislocation and noisy environment produced spurious single forces in MT+SF solution, we investigated the possibility of neglecting the forces in our inversions, i.e. inverting for the MT solution only, even if actual single forces are present in the source. We used two

mechanisms, a pure volumetric source and a vertical crack, both with a strong horizontal single force (west-east direction). In both cases the solutions for the MT were correct. In the MT+SF solutions, the moment tensor part and the true single force are correct, while spurious single forces are generated on the other single force components. The same results are obtained using a strong vertical input force.

From the obtained results we can affirm that spurious single forces are easily generated under conditions common on volcanoes, such as noisy data and mislocated source positions. Hence, particular care should be taken when interpreting the forces obtained from the inversion of real data. On the contrary, for the station configuration in this study, the MT solutions are always correct in the tests made, even if the actual single forces are neglected in the inversion. This leads us to the conclusion that, in the presence of a well constrained velocity model, MT solutions can be trusted even when noisy data are used in the inversion and that real forces, if present, will not affect this solution. It is important to note that the latter result is valid for Arenal volcano with this station distribution but cannot be generalized for all volcanoes. Separate tests for each specific site and station distribution should be performed. Performing these synthetic tests using the station distribution from the 2005 seismic installation provides us with better understanding of how different uncertainties in our data map onto the moment tensor solution. This will allow us to reliably interpret the results from the inversion of the real data catalogue. An example of an inversion of a single explosive event recorded in February 2005 is presented in the following section.

6. Application to real data

During a seismic experiment, carried out from the 10th to the 21st of February 2005, nine Güralp CMG40T seismometers, with mini-Titan recorders were deployed on Arenal volcano. This temporary network recorded several events per day. From this database a signal accompanying an explosion, occurring on the 14th of February at 21.40, was selected for moment tensor inversion (Figure 10).

Métaxian et al. (2002) and Lesage et al. (2006) reported on signals recorded during previous experiments carried out on Arenal in 1997. These signals, coming from the same source region, have durations of only 7 s (e. g. path effects are not longer than 7 s), which suggests that our 100 s long signals do not only represent path effects, but rather a complicated source process or an amalgamation of several processes. This is apparent from the spectrogram in Figure 10, where the onset of the signal has a broad spectrum followed by the separated spectral lines. These lines could be interpreted as a harmonic tremor triggered by an initial disturbance (Lesage et al., 2006). Although we consider our velocity model as a reasonable approximation of the real structure, even small uncertainties can prevent us from correctly inverting for such a long signal. This is because uncertainties in the velocity model will primarily change the coda of the signal, so in the case of a long source process this error accumulates with the time. For these reasons, we will invert for the "trigger" part of the signal only. In order to analyze how, and if, time-windowing of the signal influences our inversion we perform an additional synthetic test. In this test we simulate an explosive mechanism (no single forces are

included) using synthetic signals generated by a 40 second long source time function. The inversion is performed for the moment tensor components and moment tensor component plus single forces for a source located 200 m under the crater summit. The duration of both Green's functions and signals are reduced in the inversion code to 15 seconds and tapered. Figure 11 shows the solutions for the MT+SF (left panel) and the MT (right panel). In the solution for moment tensor components plus single forces, spurious single forces are generated along the horizontal and vertical directions. The moment tensor components for both solutions (with and without single forces allowed in the inversion) are analyzed with the principal components analysis (Vasco, 1989). This analysis is based on the singular value decomposition of the moment tensor components. Both solutions are found to consist of 94% isotropic components. The amplitude of the source time function is well retrieved by the inversion. This leads us to the conclusion that the retrieval of the correct source mechanism is not influenced by reducing the length of the signal and by using only the initial trace of the event.

To perform the inversion on the recorded event, after the deconvolution for instrument responses, the data is converted from velocity to displacement measurements. The energy peak is between 0.8 - 2 Hz, thus the signals are filtered within this band. The quality of the inversion is again evaluated through the analysis of the misfit R. Solutions for moment tensor components plus single forces, and moment tensor components only, are analyzed. Nine stations have been utilized in the inversion. The location of the source is constrained through the inversion procedure performing a grid search within the volume of possible source points. The dimensions and location of the source volume were

restricted to possible locations identified in previous work carried out on Arenal (Hagerty et al., 2000; Métaxian et al., 2002), according to which the source is likely to be located in a small area with a radius of 0.3 km around the crater summit and at a depth of no more than 600 meters. The values of the misfit are evaluated for accuracy of the solution; the best is defined by the lowest misfit. Only misfits lower than 0.5 have been considered. The low misfits are mostly concentrated in the north-west corner of our volume. Small variations of the source position inside this volume do not alter the inversion results. This was also seen with the source mislocation synthetic tests. Calculated and observed data are compared in Figure 12 while the results of the inversion are shown in Figure 13. Single forces, generated in east-west, north-south, and vertical direction appear in the solution. F_z has a larger amplitude than F_x and F_y. Our synthetic tests demonstrated that spurious single forces are easily generated with this station configuration. Therefore, given the synthetic results, we cannot be sure if they are real or spurious. Furthermore, we have shown that the solution for moment tensor components is relatively stable. For these reasons we have concentrated on the solution for MT only, analyzing it using the principal components analysis. The results give a strong isotropic component (87%) with a small percentage of compensate linear vector dipoles (CLVD) (9%) and double couple components (4%). Since our previous test showed spurious off-diagonal components, we may not rely on the deviatoric part of the solution. These results lead us to the conclusion that the mechanism generating this event is, as expected, an explosion. Assuming that the shear modulus (μ) is 10 GPa, the estimated volume change (ΔV) associated with this explosive event is 68 m^3 ($\Delta V = \mu M_o$ where M_o is the scalar seismic moment). The source position was located at roughly 200 meters beneath the crater summit. Following the

approach of Jolly et al. (2010), we performed the inversion for different source depths; the isotropic component percentage remains stable inside the source location volume with a maximum value of 85%, but the relative percentage of CLVD and double couple changes. Therefore, given the results from the synthetic tests, and considering that an inversion of the explosive event produces an isotropic solution, we are confident that the MT inversion can be applied to the data recorded during this deployment.

7. Conclusions

In this paper we present synthetic tests performed to examine how the errors involved in the moment tensor inversion influence the correct retrieval of the source time function and mechanism in the volcanic setting of Arenal volcano. In particular we focus our attention on how the signal-to-noise-ratio, and a mislocated source position, influence the results of the inversion performed for moment tensor components and moment tensor components plus single forces. We show that spurious single forces are easily generated when noisy data and mislocated source positions are included in the inversion. However, we find that the inversion for MT only gives the correct MT components of the solution even when the actual single forces are present in the source. This suggests that for this volcano, and this station configuration, we should be careful in attaching physical meaning to single forces. This information is used in the interpretation of the results of an inversion for an explosive event recorded on Arenal in 2005. Analyzing the solution with the principal components analysis of Vasco (1989), we are able to recover a predominantly explosive mechanism for the analyzed event. Performing the inversion for

different source depth shows the stability of the isotropic component present in the solution. This allows us to confidently invert for the different classes of data recorded on Arenal in 2005 in order to retrieve and compare the source mechanisms generating a range of observed events.

Acknowledgements

This work has been funded by Science Foundation Ireland (SFI). The authors wish to acknowledge the Irish Centre for High-End Computing (ICHEC) for providing computational facilities. We would also like to thank Dr Louis De Barros and Dr Shane Tyrrell for useful comments on the manuscript. The fieldwork was partly supported by the European Commission, 6th Framework Project – 'VOLUME', Contract No. 018471, INSU-CNRS (ACI Risques naturels et changements climatiques), Université de Savoie (BQR B2005-09), and projects n° 113-A6-503 and 113-A7-511 from Universidad de Costa Rica and Instituto Costarricense de Electricidad. We thank the staff of Escuela Centroamericana de Geología, Universidad de Costa Rica, and Instituto Costarricense de Electricidad for their efficient logistical support. We would also like to thank P. Jousset and an anonymous reviewer for detailed reviews which greatly improved the manuscript.

References

Aki, K. & Richards, P. G, 2002. Quantitative Seismology, 2nd ed., University Science Books, Sausalito, California, 700 pp.

Alvarado, G., Barquero, R., 1997. Las señales sísmicas del volcán Arenal (Costa Rica) y su relación con las fases eruptivas (1968–1986). Ciencia e Tecnologia, 11 (1), 15–35.

Bean, C., Lokmer, I., O'Brien, G., 2008. The influence of near-surface on long-period (LP) seismic signals and on moment tensor inversions: Simulated examples from Mt. Etna. Journal of Geophysical Research, 113, B08308, doi:10.1029/2007JB005468.

Benoit, J.P. and McNutt, S.R., 1997. New constraints on source processes of volcanic tremor at Arenal Volcano, Costa Rica, using broad-band seismic data. Geophysical Research Letters, 24, 449-452.

Chouet, B. A., 1996. Long-period volcano seismicity: its source and use in eruption forecasting. Nature, 380, 309-316.

Chouet, B. A., 2003. Volcano Seismology. Pure and Applied Geophysics, 160 (3), 739-788.

Hagerty, M.T., Schwartz, S.Y., Garcés, M.A., Protti, M., 2000. Analysis of seismic and acoustic observations at Arenal volcano, Costa Rica, 1995–1997. Journal of Volcanology and Geothermal researchResearch, 101, 27-65.

Jolly, A., Sherburn, S., Jousset, P., and Kilgour, G., 2010. Eruption source processes

521 derived from seismic and acoustic observations of the 25 September 2007 Ruapehu
522 eruption North Island, New Zealand. Journal of Volcanology and Geothermal Research,
523 191, 33–45.
524
525 Jousset, P., Neuberg, J., and Jolly, A., 2004. Modelling low-frequency earthquakes in
526 a viscoelastic medium with topography. Geophysical Journal International, 159, 776–802.
527
528 Lesage, P., Mora, M.M, Alvarado, G., Pacheco, J., Métaxian, J. P., 2006. Complex
529 behavior and source model of the tremor at Arenal volcano, Costa Rica. Journal of
530 Volcanology and Geothermal Research, 157, 49–59.
531
532 Lokmer, I., Bean, C.J., Saccorotti, G., Patanè, D., 2007. Moment tensor inversion of LP
533 events recorded on Etna in 2004 using constraints obtained from wave simulation tests.
534 Geophysical Research Letters, 34, L.22316, doi:10.1029/2007GL031902.
535
536 Lokmer, I., 2008. Long period seismic activity and moment tensor inversion in volcanic
537 environments: Application to Mount Etna. Unpublished Ph.D. Thesis, University College
538 Dublin, Ireland.
539
540 Lokmer, I., Saccorotti, G., Di Lieto, B., Bean, C. J., 2008. Temporal evolution of long-
541 period seismicity at Etna Volcano, Italy, and its relationships with the 2004-2005
542 eruption. Earth and Planetary Science Letters, 266, 205-220.
543

McNutt, S. R. (2005). Volcanic Seismology. Annual Review of Earth and Planetary Sciences, 33 (1)**,** 461-491, doi:10.1146/annurev.earth.33.092203.122459.

Menke, W., 1984. Geophysical data analysis: Discrete inverse theory. First edition, Academic Press Inc., Orlando, Florida, 260 pp.

Métaxian, J.P., Lesage, P., Dorel, J., 1997. Permanent tremor of Masaya volcano, Nicaragua: wavefield analysis and source location. Journal of Geophysical Research, 102, 22529– 22545.

Métaxian, J.P., Lesage, P., Valette, B., 2002. Locating sources of volcanic tremor and emergent events by seismic triangulation: Application to Arenal volcano, Costa Rica. Journal of Geophysical Research, 107, B10, 2243, doi:10.1029/2001JB000559.

Métaxian, J.P., O'Brien, G.S., Bean, C.J., Valette, B., Mora, M., 2009. Locating volcano-seismic signals in the presence of rough topography: wave simulations on Arenal volcano, Costa Rica. Geophysical Journal International, 179, 3, doi: 10.1111/j.1365-246X.2009.04364.x

Mora, M.M, Lesage, P., Dorel, J., Bard, P., Metaxian, J.P., Alvarado G. E., Leandro C., 2001. Study of seismic effects using H/V spectral ratios at Arenal Volcano, Costa Rica. Geophysical Research Letters, 28, n.15, 2991-2994.

Mora, M.M., Lesage, P., Valette, B., Alvarado, G.E., Leandro, C., Metaxian, J. P., Dorel, J., 2006. Shallow velocity structure and seismic site effects at Arenal volcano, Costa Rica. Journal of Volcanology and Geothermal Research, 152, 121-139.

Neuberg, J. and Pointer, T., 2000. Effects of volcano-topography on seismic broadband waveforms. Geophysical Journal International, 143, 239–248.

Neuberg, J., Luckett, R., Baptie, B., and Olsen, K., 2000. Models of tremor and low-frequency earthquake swarms on Montserrat. Journal of Volcanology and Geothermal Research, 101, 83–104.

O'Brien, G. S., Bean, C. J., 2004. A 3D discrete numerical elastic lattice method for seismic wave propagation in heterogeneous media with topography. Geophysical Research Letters, 31, L14608, doi:10.1029/2004GL020069.

Ohminato, T. and Chouet, B., 1997. A free-surface boundary condition for inclusing 3D topography in the finite-difference method. Bulletin of the Seismological Society of America, 87(2), 494–515

Ohminato, T., Chouet, B. A., Dawson, P., Kedar, S., 1998, Waveform inversion of very long period impulsive signals associated with magmatic injection beneath Kilauea Volcano, Hawaii. Journal of Geophysical Research, 103 (B10)**,** 23839-23862

590 Soto, G.J., Alvarado, G.E., 2006. Eruptive history of Arenal Volcano, Costa Rica, 7 ka to
591 present. Journal of Volcanology and Geothermal Research, 157, 254-269.
592
593 Takei, Y. & Kumazawa, M., (1994). Why have the single force and torque been
594 excluded from seismic source models? Geophysical Journal International, 118 (1), 20-30.
595
596 Vasco, D. W., (1989). Deriving source-time functions using principal component
597 analysis, Bulletin of the Seismological Society of America, 79 (3), 711-730.
598
599 Williams-Jones, G., Stix, J., Heiligmann, M., Barquero, J., Fernandez, E., Gonzalez,
600 E.D., 2001. A model of degassing and seismicity at Arenal volcano, Costa Rica. Journal
601 of Volcanology and Geothermal Research, 108, 121–139.
602
603 **Figures captions**
604
605 Figure 1. Digital elevation model and station configuration used in our synthetic tests.
606 Arenal location is shown in the right-hand panel. The triangles represent the locations of
607 the stations deployed on Arenal during a seismic experiment carried out in 2005.
608
609 Figure 2. 1D velocity model used for Arenal. The blue and red lines indicate the P-wave
610 (V_p) and S-wave (V_s) velocities versus depth, respectively.
611

Figure 3. Ricker wavelet source time function (amplitude expressed in 10^{-12} Nm) used to generate synthetic signals (top panel) and its spectrum (bottom panel).

Figure 4. Moment tensor component plus single forces solution (left panel) and moment tensor components solution (right panel) for synthetic data generated with an explosive mechanism and the Ricker wavelet source time function shown in Figure 4.

Figure 5. Moment tensor component plus single forces solution (left panel) and moment tensor components solution (right panel) obtained when random noise is added to the synthetic data (noise amplitude is equal to $1/10^{th}$ of the signal amplitude). Spurious single forces are generated in the solution for moment tensor components plus single forces. The correct solution should be: $F_x = 0$; $F_y = 0$; $F_z = 0$; $M_{xx} = 1$; $M_{yy} = 1$; $M_{zz} = 1$; $M_{xy} = 0$; $M_{xz} = 0$; $M_{yz} = 0$.

Figure 6. Same as Figure 5, with noise amplitude equal to 1/2 of the signal amplitude. Spurious single forces are generated in the solution for moment tensor components plus single forces, strongly affecting the MT+SF solution.

Figure 7. As Figure 5 (noise amplitude equal to $1/10^{th}$ of the signal amplitude). In this case, a pure volumetric source geometry with a single force was simulated. The real force is correctly retrieved while spurious single forces are generated in the other direction. The correct solution should be: $F_x = 2$; $F_y = 0$; $F_z = 0$; $M_{xx} = 1$; $M_{yy} = 1$; $M_{zz} = 1$; $M_{xy} = 0$; $M_{xz} = 0$; $M_{yz} = 0$.

635

636 Figure 8. As Figure 5 (noise amplitude equal to $1/10^{th}$ of the signal amplitude) for a crack
637 plus single force source. The real force is correctly retrieved while spurious single forces
638 are generated in the other directions. The correct solution should be: $F_x = 2$; $F_y = 0$; $F_z = 0$;
639 $M_{xx} = 2$; $M_{yy} = 1$; $M_{zz} = 1$; $M_{xy} = 0$; $M_{xz} = 0$; $M_{yz} = 0$ (moment tensor inversion for vertical
640 crack with $\lambda = 2\mu$ where λ and μ are the Lamé parameters) .

641

642 Figure 9. Same as Figure 5 (noise amplitude equal to $1/10^{th}$ of the signal amplitude) for
643 an incorrect source position. The mislocated source position does not affect the solution
644 for moment tensor components. The correct time solution should be: $F_x = 0$; $F_y = 0$; $F_z =$
645 0; $M_{xx} = 1$; $M_{yy} = 1$; $M_{zz} = 1$; $M_{xy} = 0$; $M_{xz} = 0$; $M_{yz} = 0$.

646

647 Figure 10. Explosion recorded on 14^{th} February, 2005 at 21.40. On the left, the original
648 waveform (top panel), spectrogram (middle panel) and filtered (0.8-2 Hz) waveform
649 (bottom panel) are shown. The black rectangle highlights the portion of the signal for
650 which we performed the moment tensor inversion.

651

652 Figure 11. Moment tensor component plus single forces solution (left panel) and moment
653 tensor components solution (right panel) obtained using a 40 second long source time
654 function (see text for details). The top right panel shows the original source time function
655 of 40 s. The black rectangle highlights the portion of the source used in the inversion.

656

Figure 12. Calculated (red line) and observed seismogram (blue line) are compared for the waveform inversion of the explosion that occurred on the 14th February 2005 at 21.40 (amplitude expressed in 10^{-4} m).

Figure 13. Moment tensor component plus single forces solution (left panel) and moment tensor components solution (right panel) obtained by waveform inversion of the explosion that occurred on the 14th February 2005 at 21.40.

Table 1. The values of the misfit (R) obtained for the synthetic tests and for the inversion of the explosive event that occurred on the 14th of February 2005, are listed for both moment tensor components, solutions and moment tensor components plus single forces solutions.

Moment tensor inversion of Explosive Long Period events recorded on Arenal Volcano, Costa Rica, constrained by synthetic tests.

R. Davi[1], G.S. O'Brien[1, 2], I. Lokmer[1, 2], C.J. Bean[1, 2], P. Lesage[3], M.M. Mora.[4]

[1]Seismology and Computational Rock Physics Laboratory, School of Geological Sciences, University College Dublin, Belfield, Dublin 4, Ireland.

[2]Complex and Adaptive Systems Laboratory (CASL), University College Dublin, Belfield, Dublin 4, Ireland.

[3]Laboratoire de Géophysique Interne et Tectonophysique, CNRS, Université de Savoie, 73376 Le Bourget-du-Lac Cedex, France

[4]Escuela Centroamericana de Geología, Universidad de Costa Rica, Ciudad Universitaria Rodrigo Facio, San Pedro de Montes de Oca, 214-2060 San José, Costa Rica.

Abstract

In order to constrain the moment tensor solution of an explosive seismic event recorded on Arenal volcano, Costa Rica, we perform tests using synthetic data. These data are generated using a 3D model including the topography of the volcano and the best estimation of the velocity model available for Arenal. Solutions for (i) the moment tensor components, and (ii) the moment tensor plus single forces, are analysed. When noisy data and mislocated sources are used in the inversion, spurious single forces are easily

generated in the solution for the moment tensor components plus single forces. Forces also appear when the inversion is performed using an explosive event recorded on Arenal in 2005. Synthetic tests indicate that these forces might be spurious. However the mechanism is correctly retrieved by the inversion in both solutions. The ability to recover the explosive mechanism for the 2005 event combined with the interpretative aids from the synthetics tests will enable us to invert for the large variation in events observed on Arenal.

Keywords: Arenal volcano, moment tensor inversion, single forces, synthetic tests

1. Introduction

Volcanoes are complex and challenging environments showing a great variety of behaviour. A range of earthquake types are regularly recorded on volcanoes. They include: high frequency tectonic-like events, ~~(~~ also known as volcano tectonic events, (VT), explosions, long period events (LP) and tremor. VT events have energy in the range of 2-20 Hz with very similar signatures to tectonic earthquakes. They are due to brittle rock failure, generated by regional tectonic forces, dyke propagation or pore over-pressure (McNutt, 2005). LP events and tremor are normally characterized by strongly peaked spectra. Their energy is concentrated between 0.2 and 5 Hz and they are thought to be caused by fluid movements inside volcanic conduits (Chouet, 2003). Since tremor and LP events seem to have common characteristics, differing only in duration, some authors believe they share the same source mechanism (Chouet, 1996; Neuberg et al.,

2000). These types of events often precede and accompany volcanic eruptions, hence a deeper knowledge of their source origin may be helpful in volcanic event forecasting. One of the most common tools used to retrieve the seismic source mechanism is a moment tensor inversion. The combination of moment tensor components represents a system of equivalent forces that produces the same wavefield as the actual physical processes at the source. Inverting for the seismic source mechanism has become a common procedure. Inversions for very long period events (VLP) have been successfully performed (Ohminato et al., 1998; Chouet et al., 2003) as the very long wavelengths are not influenced by structural heterogeneities. However, this is not always the case for inversions of LP events. The shortest wavelengths are sensitive to velocity structures and strong topographic effects (Bean et al., 2008; Lokmer et al., 2007; Lokmer et al., 2008; Métaxian et al., 2009). Such effects introduce many uncertainties in the inversion procedure that can lead to apparently stable, but erroneous solutions (Bean et al., 2008). In fact, due to the complexity of volcanic environments (e.g. the lack of sufficient structural information, the high degree of heterogeneity and the scattering effects due to the pronounced topography), it is quite difficult to recover a unique (and correct) source mechanism. The inclusion of single forces in the inversion procedure makes the recovery of the source mechanism an even more challenging task. However, single forces may be common in volcanic environments and have been modelled in other seismic source studies. Takei and ~~Kumarawa~~ Kumazawa (1994) provide a theoretical justification for the physical existence of these forces. However, an accurate quantification of these forces is not available at present. This is due to the fact that an inversion procedure with an

increased numbers of free parameters is extremely sensitive to uncertainties in the near-surface velocity model (Bean et al., 2008).

In this paper, we perform a moment tensor inversion of an explosive event recorded in 2005 on Arenal volcano, Costa Rica, using constraints obtained by synthetic tests. Topographical and structural effects are reduced using the best estimation of velocity model available for Arenal volcano and Green's functions are calculated including 15 m resolution digital elevation model ~~the real topography of~~of the volcano. In the synthetic tests we ~~constrain~~ assess our ability to retrieve the correct source time function and mechanism when (i) random noise is added to the data, and (ii) the source location is not accurately known. We also investigate how the presence of single forces affects the moment tensor solution. We aim to quantify our ability to accurately recover the true source from ~~a~~ real seismic data. ~~world situation.~~ The information obtained by performing the synthetic tests is used in the analysis and interpretation of the solution of the inversion performed on real explosion data from Arenal. The methodology used in the calculation of the Green's functions, and in the inversion method, is provided herein. Results of our synthetic tests, the inversion of the real event and the interpretation of the mechanism that generates this event are also presented.

2. Arenal volcano

Arenal is a small strato-volcano located in north-western Costa Rica and is mainly composed of tephra and lava flows (Soto and Alvarado, 2006); its location and

~~topography~~ digital elevation model are shown in Figure 1. It was dormant for several centuries until July 1968 when a Peléan eruption resulted in 78 fatalities and opened three new craters in the western flank. Arenal's explosive activity is still ongoing today and is preceded, and accompanied, by different types of seismic events. The most common types are LP events, explosions, spasmodic and harmonic tremor, rockfalls and sporadic volcano tectonic swarms (Alvarado and Barquero~~et al.~~, 1997). Explosions and LP events have the same frequency range (1-3 Hz), but differ in amplitude. Explosions have larger amplitudes and are accompanied by a large, audible air-shock. The explosion coda often evolves into tremor (Hagerty et al., 2000). Tremor is the most common type of event at Arenal with a duration that can last for several hours and comprises spasmodic and harmonic. Harmonic tremor can be distinguished from spasmodic tremor by their regularly spaced frequency peaks with most of the energy concentrated between 0.9 and 2 Hz. Spasmodic tremor energy spans 1-6 Hz. There is no clear difference in the genesis of spasmodic and harmonic tremor; the former can progressively evolve into the latter and vice-versa (Lesage et al., 2006). Most of the tremor exhibits a progressive gliding in frequency that can last tens to hundreds of seconds. The gliding phenomenon can be generated by pressure changes in the fluid inside the conduit (Hagerty et al., 2000). The number of seismic events can be variable during the day. However, in recent decades a decrease in the number and amplitude of explosions has been recognised (Lesage et al., 2006). Arenal's seismicity is often accompanied by gas emissions produced during the explosions and by passive degassing in rhythmic pulses along the edge of the crater (William–Jones et al., 2001). The origin of these seismic events is, at present, not fully understood.

3. Methodology

The elastic Green's functions are defined as the Earth's response to an impulsive source generated at a certain point (source location) and propagating to a receiver location in an elastic Earth. The n^{th}-component of the displacement, recorded at position $\mathbf{x}$ and time t, can be written as (Aki and Richards, 2002):

$$u_n(\mathbf{x},t) = M_{pq}(t) * G_{np,q}(\mathbf{x},t) + F_p(t) * G_{np}(\mathbf{x},t), \qquad \text{n, p, q} = 1, 2, 3 \qquad (1)$$

where M_{pq} is the force couple or dipole in the pq direction acting at the source, F_p is the single force acting in the p direction, and G_{np} and $G_{np,q}$ represent the n^{th} components of the corresponding medium responses (Green's functions) and their derivatives, respectively. The asterisk indicates convolution and the summation convention applies. Volcanoes are the most "promising" environments in which single forces are likely to be found (Takei and Kumazawa, 1994), even if the existence of these single forces in the LP process is, at present, not reliably constrained by experiments or observations. For VLP events, Chouet (2003) attributes single forces to gravitational energy in the source volume due to the ascent of a slug of gas in the volcanic conduit or by a volcanic jet during an explosion. The latter phenomenon was also successfully modelled using single forces in the recent work of Jolly et al. (2010). The reliability of the inversion results are strongly dependent on the accuracy with which the Green's functions are calculated (Lokmer, 2008). In the past, due to computational restrictions, Green's functions were

Field Code Changed

calculated only for a homogeneous half-space excluding topography. This approach leads to misinterpretations because the seismic wavefield is sensitive to layered velocity models and strongly affected by topographical scattering (Bean et al., 2008). However, in the past decade, topography has been included in the calculation of Green's functions (Ohimanto and Chouet, 2007; Neuber and Pointer, 2000; Jousset et al., 2004; Jolly et al, 2010). To avoid incorrect interpretations we require detailed information about the medium i.e. a precise velocity model or near-accurate Green's functions relative to the frequencies of interest. At present, detailed velocity models with structural information, particularly related to the layers close to the surface, are extremely rare on volcanoes due to the considerable cost and effort involved in producing such high resolution velocity models. Therefore, synthetic tests provide a powerful tool for constraining the inversion results and improving the reliability of such interpretations.

To calculate the Green's functions we use 3D-full wavefield numerical simulations including topography and the "best" estimate of the velocity structure retrieved from sounding using the spatial autocorrelation (SPAC) method, Métaxian et al., 1997, -and seismic refraction experiments carried out on Arenal in 1997 (Mora et al., 2006). In this study, we use the 3D Elastic Lattice Method (ELM), to simulate wave propagation in the elastic medium (O'Brien and Bean, 2004). To calculate the Green's functions we use a 1-D velocity model~~, see~~ (Figure 2). This velocity model comprises two major layers following the profile of the topography above a half space medium with velocities of 3.5 km/s for the P-waves (V_p) and 2.0 km/s for the S-waves (V_s) and a maximum density equal to 2500 kg/m^3. The numerical domain consists of a 13 x 11 x 6 km^3 space where

topography is derived from the Digital Elevation Model (DEM) of the volcano using a spatial grid step of 15 m. Long wavelengths are simulated using a model of large extent ~~of the model and~~with relatively small grid-step. Absorbing boundaries, 900 m thick, are included in the model to avoid edge reflections and ensure the absorption of the longest wavelengths. The top boundary of the model is a free surface including topography. To calculate the Green's functions library for a large number of source locations within a predefined source region, we adopt the Reciprocity Theorem (e.g. Aki and Richards, 2002). Green's functions are calculated over a volume (480 x 300 x 840 m^3) of 4735 points located under the crater summit. In addition to calculating the Green's functions for each single point source, we also required their spatial derivatives around the source position. Spatial derivatives can be extracted directly from the output of the simulation and are given by the central finite-difference derivative

$$G_{np,q}(\mathbf{r},\mathbf{s}) \approx \frac{G_{np}(\mathbf{r},\mathbf{s}+\Delta q) - G_{np}(\mathbf{r},\mathbf{s}-\Delta q)}{2\Delta q} \qquad (2)$$

where $G_{np,q}(\mathbf{r},\mathbf{s})$ is the spatial derivative of the Green's functions G_{np} around the source position, $\mathbf{s}$ is the source position, $\mathbf{r}$ is the receiver position and Δq is the spatial grid spacing. The Green's functions were calculated using a Gaussian source time function with ~~for~~ a frequency range of up to 5 Hz and a duration of 15 s. The recording positions for the synthetic data map to the real locations of nine stations deployed on the volcano during a seismic experiment carried out in February 2005, as shown in Figure ~~3~~1. Since Arenal is quite a dangerous environment (due to the frequent pyroclastic flows and the

ballistic bombardment of blocks and bombs), the stations were deployed on the flanks of the volcano but, unfortunately, could not be placed close to the summit.

In the frequency domain ~~without the single forces term~~, equation (1) can be written as:

$$u_n(\mathbf{x}, \omega) = M_{pq}(\omega) G_{np,q}(\mathbf{x}, \omega) + G_{np}(\mathbf{x}, \omega) F_p(\omega) \quad (3)$$

where $u_n(\omega)$, $M_{pq}(\omega)$, $F_p(\omega)$, $G_{np}(\omega)$, $G_{np,q}(\omega)$, are the spectra of the displacements, of the moment tensor components, of the single forces and ~~and~~ of the components and of the spatial derivatives of the Green's functions, respectively. The equation is solved separately for each frequency. The results are then transformed into the time domain using an inverse Fourier Transform. Equation (3) can be written in matrix form as:

$$\mathbf{u} = \mathbf{Gm} \quad (4)$$

where **u** is the data matrix, **G** is matrix containing the Green's functions and derivatives, **m** is the moment tensor and single forces components' matrix. If N is the number of seismograms used in the inversion, equation 4 can be also written in an explicit form as;

202 $$\begin{bmatrix} u_1 \\ u_2 \\ \cdot \\ \cdot \\ \cdot \\ u_N \end{bmatrix} = \begin{bmatrix} g_{11,1} & g_{12,2} & g_{13,3} & g_{11,2} & g_{11,3} & g_{12,3} & g_{11} & g_{12} & g_{13} \\ g_{21,1} & g_{22,2} & g_{23,3} & g_{21,2} & g_{21,3} & g_{22,3} & g_{21} & g_{22} & g_{23} \\ g_{31,1} & g_{32,2} & g_{33,3} & g_{31,2} & g_{31,3} & g_{32,3} & g_{31} & g_{32} & g_{33} \\ \vdots & \vdots & \vdots & \vdots & \vdots & \vdots & \vdots & \vdots & \vdots \\ \vdots & \vdots & \vdots & \vdots & \vdots & \vdots & \vdots & \vdots & \vdots \\ g_{N1,1} & g_{N2,2} & g_{N3,3} & g_{N1,2} & g_{N1,3} & g_{N2,3} & g_{N1} & g_{N2} & g_{N3} \end{bmatrix} \cdot \begin{bmatrix} M_{11} \\ M_{22} \\ M_{33} \\ M_{12} \\ M_{13} \\ M_{23} \\ F_1 \\ F_2 \\ F_3 \end{bmatrix} \quad (5)$$

203

204 with the assumption (due to the symmetry of the moment tensor) that

205

206 $$g_{np,q} = \begin{cases} G_{np,q} & p = q \\ G_{np,q} + G_{nq,p} & p \neq q \end{cases} \qquad n = 1,2,3,..N \quad (6)$$

207

208 The quality of our inversion procedure is tested through the evaluation of the misfit (R)
209 between calculated and observed data. R can be expressed by the following equation:

210

211 $$R = \frac{(\mathbf{u} - \mathbf{Gm})^T \mathbf{W} (\mathbf{u} - \mathbf{Gm})}{\mathbf{u}^T \mathbf{W} \mathbf{u}} \quad (7)$$

212

213 where **W** is a diagonal weighting matrix of the quality of the waveforms. It can be
214 expressed in explicit matrix format as

215

$$W=\begin{bmatrix} w_1 & 0 & \cdots & 0 \\ 0 & w_2 & \cdots & 0 \\ \vdots & \vdots & \ddots & \vdots \\ 0 & 0 & \cdots & w_N \end{bmatrix} \quad (8)$$

The lowest value of the misfit R indicates the best solution for ***m***. As equation 4 is a linear equation, its least squares solution can be expressed as (Menke, 1984):

$$\mathbf{m}^{est} = \left(\mathbf{G}^T\mathbf{W}\mathbf{G}\right)^{-1}\mathbf{G}^T\mathbf{W}\mathbf{u} \quad (9)$$

where the superscript "T" denotes the transpose matrix and $\mathbf{m}^{est}$ is the estimated moment-tensor matrix. Since data recorded at different stations can show different noise signatures, the weight matrix plays an important role in the inversion procedure. ~~. A small amount of noise in the data can results in large errors in the derivation of source mechanisms, even leading to erroneous solutions. A good example of how noise can influence the retrieval of the correct solution is given by Aster et al. (2005, pp. 73-79).~~

4. Description and results of Synthetic Tests

The inversion technique is normally very sensitive to a range of effects present in volcanic environments such as those associated with topography, near surface structures and heterogeneities. To test the consistency and limitations of our inversion procedure we performed a series of synthetic tests. In these tests we attempt to (i) investigate our ability

to retrieve the correct source time function and mechanism for a fixed source location when random noise is added to our synthetic data, and (ii) analyze how a mislocated source position can influence the inversion solution while highlighting the role played by the single forces.

The use of synthetic tests is of crucial importance ~~for a~~to contribute to the ~~full~~ understanding of the inversion technique and to retrieve the correct mechanism acting on the volcano. Using 3D numerical simulations we generate synthetic signals with a Ricker wavelet source time function with a central frequency of 2 Hz, shown in Figure ~~4~~3. The source is positioned under the crater summit where the real source is most likely to be located (Benoit and McNutt, 1997; Hagerty et al., 2000; Mora et al., 2001; Lesage et al., 2006). Source locations are not fully constrained at depth but the epicenters are probably located in a small area centered under the active crater (Métaxian et al., 2002). We fix our source point at a depth of 200 meters beneath the crater summit. The mechanism simulated is an explosion ($M = 10^{12}$ Nm). No single forces are included. The inversion was performed for both a moment tensor plus single forces (MT+SF), and moment tensor only (MT).

It is important to note that in the following tests the moment tensor parts of the source solution are expressed in 10^{12} Nm, while the force parts are expressed in 10^{9} N. This is due to the fact that a force of 10^{9} N will produce ~~the same~~a displacement with the same amplitude of~~as~~ a moment of 10^{12} Nm if their radiation patterns are ignored (radiation pattern~~this~~ can be ~~done~~ ignored ~~due to~~because of the good azimuthal coverage of the

deployment). We validate (not shown here) that this holds for our station configuration, i.e. that the radiation patterns of the obtained moments and forces do not introduce significant deviation from the ~~relationship~~ general rule outlined above. Consequently, if we plot moment and forces using the same scale, forces will not be visible in the diagrams even if they ~~considerably~~ contribute~~s~~ considerably to the total amplitude of the signals.

The first test aims to show the ability of our inversion code to retrieve the exact mechanism and source time function. Since we used the exact Green's functions calculated for the exact source position, the correct solution is expected to be retrieved. Figure ~~5~~ 4 shows the results of the test for the moment tensor components plus single forces (MT+SF) in the left panel and moment tensor only (MT) in the right panel using the field location of the nine stations. Solutions are characterized by a small value of the misfit (approximately equal to zero). Since the source time function and the mechanism are perfectly recovered by the inversion, and the value of R is small, we can affirm that the correct solution is retrieved by our inversion code for both solutions (MT and MT+SF). Table 1 lists the values of the misfits of the inversions performed using synthetic and real data.

Since data recorded on volcanoes can often have a low signal-to-noise ratio, we attempt to simulate a real situation by adding noise to our synthetic data. In the frequency range of interest, we contaminate our synthetic dataset with random noise derived from the noise level of the real data recorded on Arenal. These data show a low level of

contamination of noise equally distributed at all the stations. The amplitude of the noise is within 10% of the average rms amplitude (signal-to-noise ratio, SNR = 10). The inversion is performed for the moment tensor components and the moment tensor components plus single forces. Results of the test are illustrated in Figure ~~6~~5. Spurious single forces appear in the MT+SF inversion solution. Since the amplitude of the noise is small, the solution is not dominated by the spurious forces and the source time function and explosive mechanism are correctly recovered by both inversions (see M_{xx}, M_{yy}, M_{zz} ~~diagonal~~ components for MT and MT+SF solution). In order to test how larger noise amplitudes influence the solution we increased the noise level to 50% of the average rms amplitude, which could be the case if strong tremor was recorded simultaneously with LP events. The amplitude of the spurious forces increases with the increase in noise level. As shown in Figure ~~7~~ 6 (right panel) the MT solution remains stable and correct, while in the case of MT+SF the spurious single forces strongly ~~influences~~ contaminate~~s~~ the solution. The source time function and mechanism recovered along the diagonal components of the moment tensor solution (MT+SF) are no longer correctly retrieved and the solutions do not look stable. This leads to the conclusion that noise introduces a larger error into the inversion with more free parameters.

Since spurious single forces can be generated when noisy data are used in the inversion, we want to investigate how the presence of real single forces can influence the solution. In order to understand the role played by single forces in the inversion procedure for both MT and MT+SF solution, we perform synthetic tests in which different geometries are simulated (e.g. pure volumetric source and a vertical crack with the normal parallel to the

x direction) along with including a strong single force in the ~~West~~west ~~East~~ east (x) direction. Again twelve stations have been used along with a signal to noise ratio of 10. Results for the pure volumetric source ($M = 10^{12}$ Nm) and single force ($F = 10^{9}$ N) are shown in Figure ~~8~~7. Solutions for the moment tensor components (Figure ~~8~~7, right panel) are correctly retrieved by the inversion procedure even though a real single force is included in the actual input source. In the solution for the MT+SF (Figure ~~8~~7, left panel), spurious single forces are generated in the vertical and ~~North~~north ~~South~~ south directions, in addition to larger amplitudes along the z direction. The amplitude of the ~~West~~west-~~East~~ east force is successfully retrieved, while the source-time function exhibits "ringing" in the tail of the retrieved signal. Results for a vertical crack with single ~~West~~west-~~East~~ east horizontal force are shown in Figure ~~9~~8. The MT inversion solution (Figure ~~9~~8, right panel) is well resolved, but spurious single forces are again generated for the MT+SF solution, left panel of Figure ~~9~~8. For the vertical crack the spurious force along the z direction has a slightly larger amplitude than the one generated for a pure volumetric source. For both geometries along the off-diagonal components, a small non-volumetric component is generated. The generation of this component can be considered as an artifact of the inversion procedure and it does not significantly affect the solution.

The same test has been performed using an input single force along the vertical direction. The MT solutions are correct for pure volumetric sources and vertical crack geometries. In the solution for MT+SF, the moment tensor part and the vertical force are again correctly retrieved while spurious single forces are present in the ~~North~~north ~~South~~ south and ~~West~~west-~~East~~ east directions. Since the same solutions have been obtained using a

~~West~~west-~~East~~ east and a vertical input force, only solutions for the horizontal force is presented.

Finally a test is performed to analyze how the solution of the moment tensor inversion for MT and MT+SF is influenced when an incorrect source position is used. The signal to noise ratio is again 10. With this test we aim to resemble a realistic, and quite common, situation in which the correct position of the seismic source is unknown and difficult to determine. The mislocated source is fixed in a positioned 240 m in the x-direction, 345 m in the y-direction and 500 m in the z-direction away from the correct source (located under the crater summit at a depth of 200 m). In the test, an explosive source mechanism has been simulated with no single forces included in the inversion. The solution is shown in Figure ~~10~~9. For the MT solution the explosive mechanism and the Ricker-like wavelet source time function are well retrieved by the inversion. In the MT+SF solution spurious single forces are generated, particularly in the z-direction. The amplitudes of the spurious single forces originating from a mislocated source position are comparable to the amplitudes of the forces generated when noise is added to our synthetic data (see Figure ~~6~~ 5 and ~~10~~9). This leads to the conclusion that in the presence of a noise with amplitude within 10% of the average rms, the solution is insensitive to the ~~precise~~ inaccurate location of the source.

5. Discussion of synthetic tests

We performed the synthetic tests in order to constrain the inversion of the real data from Arenal volcano. In particular, we wanted to investigate how different signal to noise ratios, and ~~wrong~~ errors in the source locations ~~of the source~~, influence the inversion solutions. We also tested the inversion code using synthetic data generated with 3D numerical simulations. We have shown that results for noisy data give stable MT solutions in which the source time function and mechanism are correctly retrieved. In the case where forces are allowed in the solutions (MT+SF), spurious single forces are generated with the largest amplitudes in the z-direction. When the signal to noise ratio decreases, the amplitude of the spurious single forces increases, strongly influencing the solution. When the signal to noise ratio is decreased to 2, the source time function and mechanism are no longer retrieved in the MT+SF solution. In addition, the spurious single forces entirely dominate the solution. Finally, we tested the sensitivity of the inversion to source mislocation. In this case the correct source time function and mechanism are correctly retrieved for the MT solution, while solutions for the MT+SF give rise to spurious single forces. Since both the source mislocation and noisy environment produced spurious single forces in MT+SF solution, we investigated the possibility of neglecting the forces in our inversions, i.e. inverting for the MT solution only, even if actual single forces are present in the source. We used two mechanisms, a pure volumetric source and a vertical crack, both with a strong horizontal single force (~~West~~west ~~East~~ east direction). In both cases the solutions for the MT were correct. In the MT+SF solutions, the moment tensor part and the true single force are correct, while spurious single forces are generated on the other single force components. The same results are obtained using a strong vertical input force.

From the obtained results we can affirm that spurious single forces are easily generated under conditions common on volcanoes, such as noisy data and mislocated source positions. Hence, particular care should be taken when interpreting the forces obtained from the inversion of real data. On the contrary, for the station configuration in this study, the MT solutions are always correct in the tests made, even if the actual single forces are neglected in the inversion. This leads us to the conclusion that, in the presence of a well constrained velocity model, MT solutions can be trusted even when noisy data are used in the inversion and that real forces, if present, will not affect this solution. It is important to note that the latter result is valid for Arenal volcano with this station distribution but cannot be generalized for all volcanoes. Separate tests for each specific site and station distribution should be performed. Performing these synthetic tests using the station distribution from the 2005 seismic installation provides us with better understanding of how different uncertainties in our data map onto the moment tensor solution. This will allow us to reliably interpret the results from the inversion of the real data catalogue. An example of an inversion of a single explosive event recorded in February 2005 is presented in the following section.

6. Application to real data

During a seismic experiment, carried out from the 10th to the 21st of February 2005, nine Güralp CMG40T seismometers, with mini-Titan recorders were deployed on Arenal volcano. This temporary network recorded several events per day. From this database a

signal accompanying an explosion, occurring on the 14th of February at 21.40, was selected for moment tensor inversion (Figure ~~11~~10).

Métaxian et al. (2002) and Lesage et al. (2006) reported on signals recorded during previous experiments carried out on Arenal in 1997. These signals, coming from the same source region, have durations of only 7 s (e. g. path effects are not longer than 7 s), which suggests that our 100 s long signals do not only represent path effects, but rather a complicated source process or an amalgamation of several processes. This is apparent from the spectrogram in Figure ~~11~~10, where the onset of the signal has a broad spectrum followed by the separated spectral lines. These lines could be interpreted as a harmonic tremor triggered by an initial disturbance (Lesage et al., 2006). Although we consider our velocity model as a reasonable approximation of the real structure, even small uncertainties can prevent us from correctly inverting for such a long signal. This is because uncertainties in the velocity model will primarily change the coda of the signal, so in the case of a long source process this error accumulates with the time. For these reasons, we will invert for the "trigger" part of the signal only. In order to analyze how, and if, ~~the~~ time-windowing of the signal influences our inversion we perform an additional synthetic test. In this test we simulate an explosive mechanism (no single forces are included) using synthetic signals generated by a 40 second long source time function. The inversion is performed for the moment tensor components and moment tensor component plus single forces for a source located 200 m under the crater summit. The duration of both Green's functions and signals are reduced in the inversion code to 15 seconds and tapered. Figure ~~12~~ 11 shows the solutions for the MT+SF (left panel) and

the MT (right panel). In the solution for moment tensor components plus single forces, spurious single forces are generated along the horizontal and vertical directions. The moment tensor components for both solutions (with and without single forces allowed in the inversion) are analyzed with the principal components analysis (Vasco, 1989). This analysis is based on the singular value decomposition of the moment tensor components. Both solutions are found to consist of 94% isotropic components. The amplitude of the source time function is well retrieved by the inversion. This leads us to the conclusion that the retrieval of the correct source mechanism is not influenced by reducing the length of the signal and by using only the initial trace of the event.

To perform the inversion on the recorded event, after the deconvolution for instrument responses, the data is converted from velocity to displacement measurements. The energy peak is between 0.8 - 2 Hz, thus the signals are filtered within this band. The quality of the inversion is again evaluated through the analysis of the misfit R. Solutions for moment tensor components plus single forces, and moment tensor components only, are analyzed. Nine stations have been utilized in the inversion. The location of the source is constrained through the inversion procedure performing a grid search within the volume of possible source points. The dimensions and location of the source volume were restricted to possible locations identified in previous work carried out on Arenal (Hagerty et al., 2000; Métaxian et al., 2002), according to which the source is likely to be located in a small area with a radius of 0.3 km around the crater summit and at a depth of no more than 600 meters. The values of the misfit are evaluated for accuracy of the solution; the best is defined by the lowest misfit. Only misfits lower than 0.5 have been considered.

The low misfits are mostly concentrated in the ~~North~~north-~~West~~ west corner of our volume. Small variations of the source position inside this volume do not alter the inversion results. This was also seen with the source mislocation synthetic tests. Calculated and observed data are compared in ~~f~~Figure ~~13~~ 12 while the results of the inversion are shown in Figure ~~14~~13. Single forces, generated in ~~East~~east-~~West~~west, ~~North~~north-~~South~~south, and vertical direction appear in the solution. F_z has a larger amplitude than F_x and F_y. Our synthetic tests demonstrated that spurious single forces are easily generated with this station configuration. Therefore, given the synthetic results, we cannot be sure if they are real or spurious. Furthermore, we have shown that the solution for moment tensor components is relatively stable. For these reasons we have concentrated on the solution for MT only, analyzing it using the principal components analysis. The results give a strong isotropic component (87%) with a small percentage of compensate linear vector dipoles (CLVD) (9%) and double couple components (4%). Since our previous test showed spurious off-diagonal components, we may not rely on the deviatoric part of the solution. These results lead us to the conclusion that the mechanism generating this event is, as expected, an explosion. Assuming that the shear modulus (μ) is 10 GPa, the estimated volume change (ΔV) associated with this explosive event is 68 m^3 ($\Delta V = \mu M_o$ where M_o is the scalar seismic moment). The source position was located at roughly 200 meters beneath the crater summit. Following the approach of Jolly et al. (2010), we performed the inversion for different source depths; ~~T~~the isotropic component percentage remains stable inside the source location volume with a maximum value of 85%, but the relative percentage of CLVD and double couple changes. Therefore, given the results from the synthetic tests, and considering that an inversion of

the explosive event produces an isotropic solution, we are confident that the MT inversion can be applied to the ~~LP~~ data recorded during this deployment.

7. Conclusions

In this paper we present synthetic tests performed to examine how the errors involved in the moment tensor inversion influence the correct retrieval of the source time function and mechanism in the volcanic setting of Arenal volcano. In particular we focus our attention on how the signal-to-noise-ratio, and a mislocated source position, influence the results of the inversion performed for moment tensor components and moment tensor components plus single forces. We show that spurious single forces are easily generated when noisy data and mislocated source positions are included in the inversion. ~~On the contrary~~However, we find that the inversion for MT only gives the correct MT components of the solution even when the actual single forces are present in the source. This suggests that for this volcano, and this station configuration, we should be careful in attaching physical meaning to single forces. This information is used in the interpretation of the results of an inversion for an explosive event recorded on Arenal in 2005. Analyzing the solution with the principal components analysis of Vasco (1989), we are able to recover a predominantly explosive mechanism for the analyzed event. Performing the inversion for different source depth shows the stability of the isotropic component present in the solution. This allows us to ~~confidentially~~ confidently invert for the ~~other~~ , different classes of data recorded on Arenal in 2005 in order to retrieve and compare the source mechanisms generating a range of observed events.

Acknowledgements

This work has been funded by Science Foundation Ireland (SFI). The authors wish to acknowledge the Irish Centre for High-End Computing (ICHEC) for providing computational facilities. We would also like to thank Dr Louis De Barros and Dr Shane Tyrrell for useful comments on the manuscript. The fieldwork was partly supported by the European Commission, 6th Framework Project – 'VOLUME', Contract No. 018471, INSU-CNRS (ACI Risques naturels et changements climatiques), Université de Savoie (BQR B2005-09), and projects n° 113-A6-503 and 113-A7-511 from Universidad de Costa Rica and Instituto Costarricense de Electricidad. We thank the staff of Escuela Centroamericana de Geología, Universidad de Costa Rica, and Instituto Costarricense de Electricidad for their efficient logistical support. We would also like to thank P. Jousset and an anonymous reviewer for detailed reviews which greatly improved the manuscript.

References

Aki, K. & Richards, P. G, 2002. Quantitative Seismology, 2nd ed., University Science Books, Sausalito, California, 700 pp.

~~Aster, R. C., Borchers, B., Thurber, C. H., 2005. Parameter Estimation and Inverse Problems. Elsevier Academic Press, 300 pp.~~

Alvarado, G., Barquero, R., 1997. Las señales sísmicas del volcán Arenal (Costa Rica) y su relación con las fases eruptivas (1968–1986). Ciencia e. Tecnol.ogia, 11 (1), 15–35.

Bean, C., Lokmer, I., O'Brien, G., 2008. The influence of near-surface on long-period (LP) seismic signals and on moment tensor inversions: Simulated examples from Mt. Etna. Journal of Geophysical Research, 113, B08308, doi:10.1029/2007JB005468.

Benioit, J.P. and McNutt, S.R., 1997. New constraints on source processes of volcanic tremor at Arenal Volcano, Costa Rica, using broad-band seismic data. Geophysical Research Letters, 24, 449-452.

Chouet, B. A., 1996. Long-period volcano seismicity: its source and use in eruption forecasting. Nature, 380., 309-316.

Chouet, B. A., 2003. Volcano Seismology. Pure and Applied Geophysics, 160 (3), 739-788.

Hagerty, M.T., Schwartz, S.Y., Garcés, M.A., Protti, M., 2000. Analysis of seismic and acoustic observations at Arenal volcano, Costa Rica, 1995–1997. Journal of Volcanology and Geothermal researchResearch, 101, 27-65.

Jolly, A., Sherburn, S., Jousset, P., and Kilgour, G., 2010. Eruption source processes derived from seismic and acoustic observations of the 25 September 2007 Ruapehu

eruption North Island, New Zealand. Journal of Volcanology and Geothermal Research, 191, 33–45.

Jousset, P., Neuberg, J., and Jolly, A., 2004. Modelling low-frequency earthquakes in a viscoelastic medium with topography. Geophysical Journal International, 159, 776–802.

Lesage, P., Mora, M.M, Alvarado, G., Pacheco, J., Métaxian, J. P., 2006. Complex behavior and source model of the tremor at Arenal volcano, Costa Rica. Journal of Volcanology and Geothermal Research, 157, 49–59.

Lokmer, I., Bean, C.J., Saccorotti, G., Patanè, D., 2007. Moment tensor inversion of LP events recorded on Etna in 2004 using constraints obtained from wave simulation tests. Geophysical Research Letters, 34, L.22316, doi:10.1029/2007GL031902.

Lokmer, I., 2008. Long period seismic activity and moment tensor inversion in volcanic environments: Application to Mount Etna. Unpublished Ph.D. Thesis, University College Dublin, Ireland.

Lokmer, I., Saccorotti, G., Di Lieto, B., Bean, C. J., 2008. Temporal evolution of long-period seismicity at Etna Volcano, Italy, and its relationships with the 2004-2005 eruption. Earth and Planet. ary Sci. ence Lett., ers, 266, 205-220.

McNutt, S. R. (2005). Volcanic Seismology. Annual Review of Earth and Planetary Sciences, 33 (1), 461-491, doi:10.1146/annurev.earth.33.092203.122459.

Menke, W., 1984. Geophysical data analysis: Discrete inverse theory. First edition, Academic Press Inc., Orlando, Florida, 260 pp.

Métaxian, J.P., Lesage, P., Dorel, J., 1997. Permanent tremor of Masaya volcano, Nicaragua: wavefield analysis and source location. Journal of Geophysical Research, 102, 22529– 22545.

Métaxian, J.P., Lesage, P., Valette, B., 2002. Locating sources of volcanic tremor and emergent events by seismic triangulation: Application to Arenal volcano, Costa Rica. Journal of Geophysical Research, 107, B10, 2243, doi:10.1029/2001JB000559.

Métaxian, J.P., O'Brien, G.S., Bean, C.J., Valette, B., Mora, M., 2009. Locating volcano-seismic signals in the presence of rough topography: wave simulations on Arenal volcano, Costa Rica. Geophysical Journal International, 179, 3, doi: 10.1111/j.1365-246X.2009.04364.x

Mora, M.M, Lesage, P., Dorel, J., Bard, P., Metaxian, J.P., Alvarado G. E., Leandro C., 2001. Study of seismic effects using H/V spectral ratios at Arenal Volcano, Costa Rica. Geophysical Research Letters, 28, n.15, 2991-2994.

Mora, M.M., Lesage, P., Valette, B., Alvarado, G.E., Leandro, C., Metaxian, J. P., Dorel, J., 2006. Shallow velocity structure and seismic site effects at Arenal volcano, Costa Rica. Journal of Volcanology and Geothermal Research, 152, 121-139.

Neuberg, J. and Pointer, T., 2000. Effects of volcano-topography on seismic broadband waveforms. Geophysical Journal International, 143, 239–248.

Neuberg, J., Luckett, R., Baptie, B., and Olsen, K., 2000. Models of tremor and low-frequency earthquake swarms on Montserrat. Journal of Volcanology and Geothermal Research, 101, 83–104.

O'Brien, G. S., Bean, C. J., 2004. A 3D discrete numerical elastic lattice method for seismic wave propagation in heterogeneous media with topography. Geophysical Research Letters, 31, L14608, doi:10.1029/2004GL020069.

Ohminato, T. and Chouet, B., 1997. A free-surface boundary condition for inclusing 3D topography in the finite-difference method. Bulletin of the Seismological Society of America, 87(2), 494–515

Ohminato, T., Chouet, B. A., Dawson, P., Kedar, S., 1998, Waveform inversion of very long period impulsive signals associated with magmatic injection beneath Kilauea Volcano, Hawaii. Journal of Geophysical. Research, 103 (B10), 23839-23862

Formatted: Don't adjust space between Asian text and numbers

Soto, G.J., Alvarado, G.E., 2006. Eruptive history of Arenal Volcano, Costa Rica, 7 ka to present. Journal of Volcanology and Geothermal Research, 157, 254-269.

Takei, Y. & Kumazawa, M., (1994). Why have the single force and torque been excluded from seismic source models?. Geophysical Journal International, 118 (1), 20-30.

Vasco, D. W., (1989). Deriving source-time functions using principal component analysis, Bulletin of the Seismological Society of America, 79 (3), 711-730.

Williams-Jones, G., Stix, J., Heiligmann, M., Barquero, J., Fernandez, E., Gonzalez, E.D., 2001. A model of degassing and seismicity at Arenal volcano, Costa Rica. Journal of Volcanology and Geothermal Research, 108, 121–139.

Figures captions

Figure 1. Digital elevation model and station configuration used in our synthetic tests. Arenal location is showedn in the right-hand panel. The triangles represent the locations of the stations deployed on Arenal during a seismic experiment carried out in 2005.

Figure 2. 1D velocity model used for Arenal. The blue and red lines indicate the P-wave (V_p) and S-wave (V_s) velocities versus depth, respectively.

~~Figure 3. used in our synthetic tests. The stars represent the locations of the stations deployed on Arenal during a seismic experiment carried out in 2005.~~

Figure ~~4~~3. Ricker wavelet source time function (amplitude expressed in 10^{-12} Nm) used to generate synthetic signals (top panel) and its spectrum (bottom panel).

Figure ~~5~~4. Moment tensor component plus single forces solution (left panel) and moment tensor components solution (right panel) for synthetic data generated with an explosive mechanism and the Ricker wavelet source time function shown in Figure 4.

Figure ~~6~~5. Moment tensor component plus single forces solution (left panel) and moment tensor components solution (right panel) obtained when random noise is added to the synthetic data (noise amplitude is equal to $1/10^{th}$ of the signal amplitude). Spurious single forces are generated in the solution for moment tensor components plus single forces. The correct solution should be: $F_x = 0$; $F_y = 0$; $F_z = 0$; $M_{xx} = 1$; $M_{yy} = 1$; $M_{zz} = 1$; $M_{xy} = 0$; $M_{xz} = 0$; $M_{yz} = 0$.

Figure ~~7~~6. Same as Figure ~~6~~5, with noise amplitude equal to 1/2 of the signal amplitude. Spurious single forces are generated in the solution for moment tensor components plus single forces, strongly affecting the MT+SF solution.

Figure ~~8~~7. As Figure ~~6~~ 5 (noise amplitude equal to 1/10th of the signal amplitude). In this case, a pure volumetric source geometry with a single force was simulated. The real force is correctly retrieved while spurious single forces are generated in the other direction. The correct solution should be: $F_x = 2$; $F_y = 0$; $F_z = 0$; $M_{xx} = 1$; $M_{yy} = 1$; $M_{zz} = 1$; $M_{xy} = 0$; $M_{xz} = 0$; $M_{yz} = 0$.

Figure ~~9~~8. As Figure ~~6~~ 5 (noise amplitude equal to 1/10th of the signal amplitude) for a crack plus single force source. The real force is correctly retrieved while spurious single forces are generated in the other directions. The correct solution should be: $F_x = 2$; $F_y = 0$; $F_z = 0$; $M_{xx} = 2$; $M_{yy} = 1$; $M_{zz} = 1$; $M_{xy} = 0$; $M_{xz} = 0$; $M_{yz} = 0$ (moment tensor inversion for vertical crack with $\lambda = 2\mu$ where λ and μ are the Lamé parameters) .

Figure ~~10~~9. Same as Figure ~~6~~ 5 (noise amplitude equal to 1/10th of the signal amplitude) for an incorrect source position. The mislocated source position does not affect the solution for moment tensor components. The correct time solution should be: $F_x = 0$; $F_y = 0$; $F_z = 0$; $M_{xx} = 1$; $M_{yy} = 1$; $M_{zz} = 1$; $M_{xy} = 0$; $M_{xz} = 0$; $M_{yz} = 0$.

Figure ~~11~~10. Explosion recorded on 14th February, 2005 at 21.40. On the left, the original waveform (top panel), spectrogram (middle panel) and filtered (0.8-2 Hz) waveform (bottom panel) are shown. The black rectangle highlights the portion of the signal for which we performed the moment tensor inversion.

Figure ~~12~~11. Moment tensor component plus single forces solution (left panel) and moment tensor components solution (right panel) obtained using a 40 second long source time function (see text for details). The top right panel shows the original source time function of 40 s. The black rectangle highlights the portion of the source used in the inversion.

Figure ~~13~~12. Calculated (red line) and observed seismogram (blue line) are compared for the waveform inversion of the explosion that occurred on the 14th February 2005 at 21.40 (amplitude expressed in 10^{-4} m).

Figure ~~14~~13. Moment tensor component plus single forces solution (left panel) and moment tensor components solution (right panel) obtained by waveform inversion of the explosion that occurred on the 14th February 2005 at 21.40.

Table 1. The values of the misfit (R) obtained for the synthetic tests and for the inversion of the explosive event that occurred on the 14th of February 2005, are listed for both moment tensor components ~~only,~~ solutions and moment tensor components plus single forces solutions.

Figure 1

Click here to download high resolution image

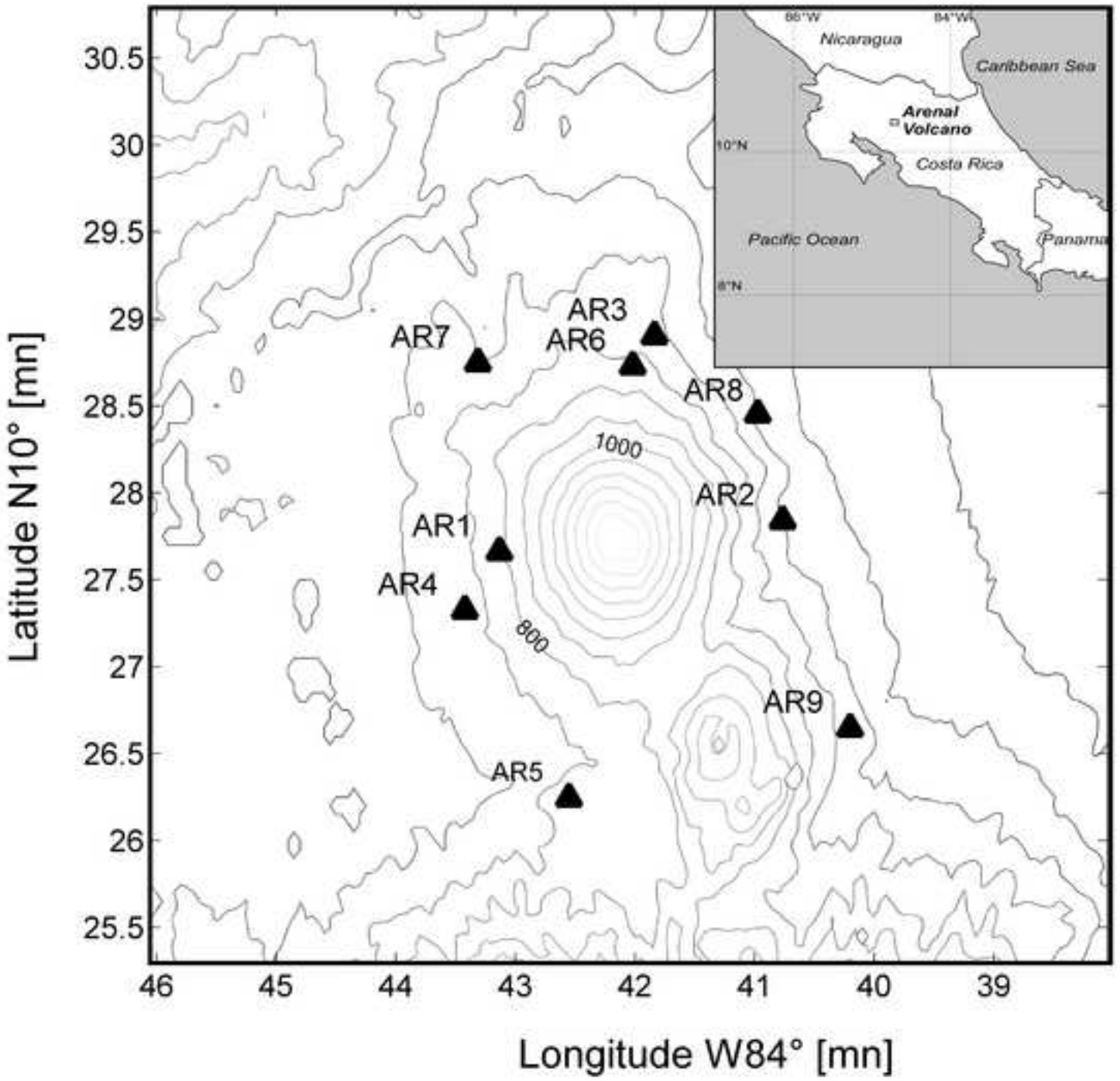

Figure 2

Click here to download high resolution image

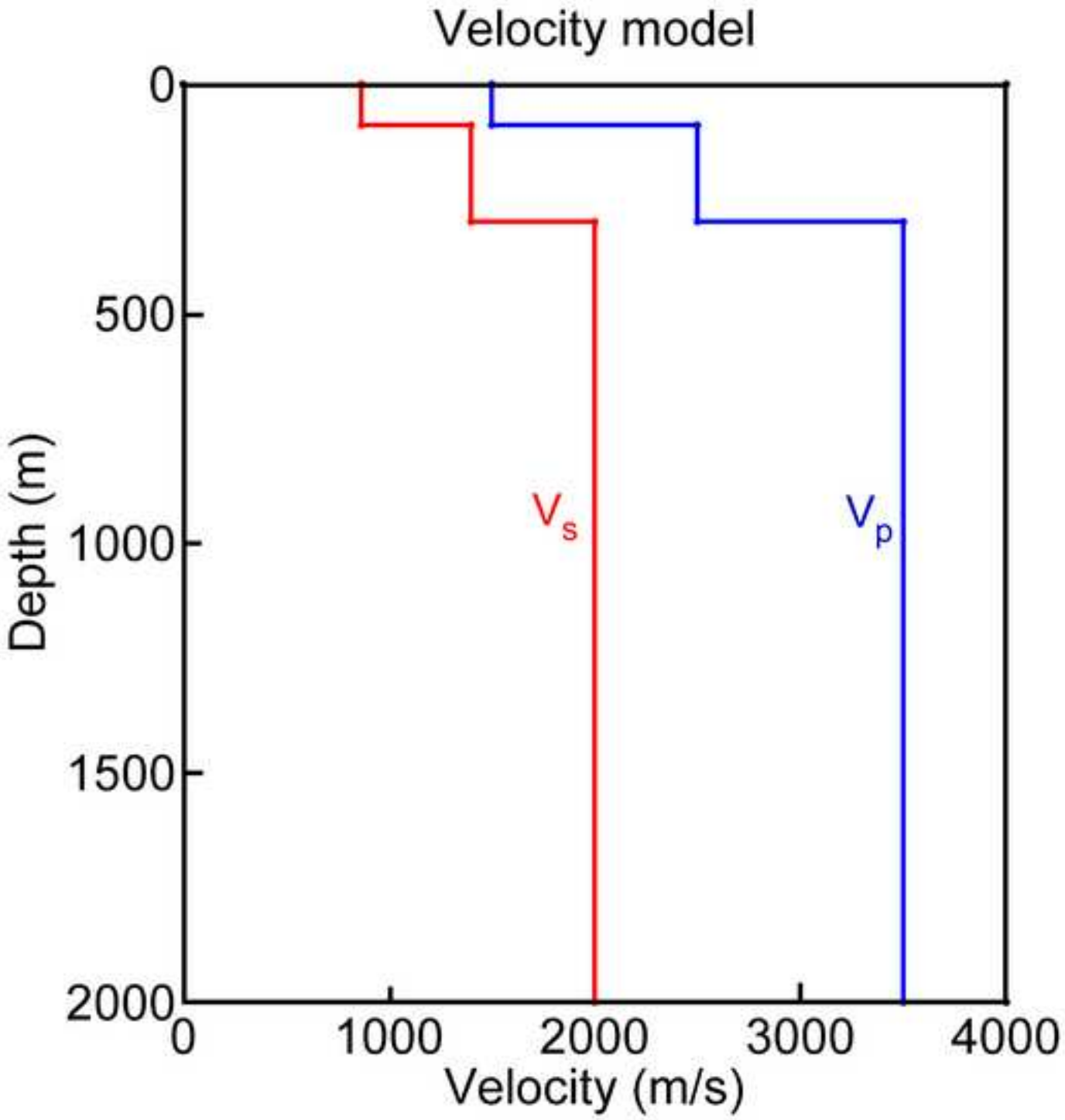

Figure 3

Click here to download high resolution image

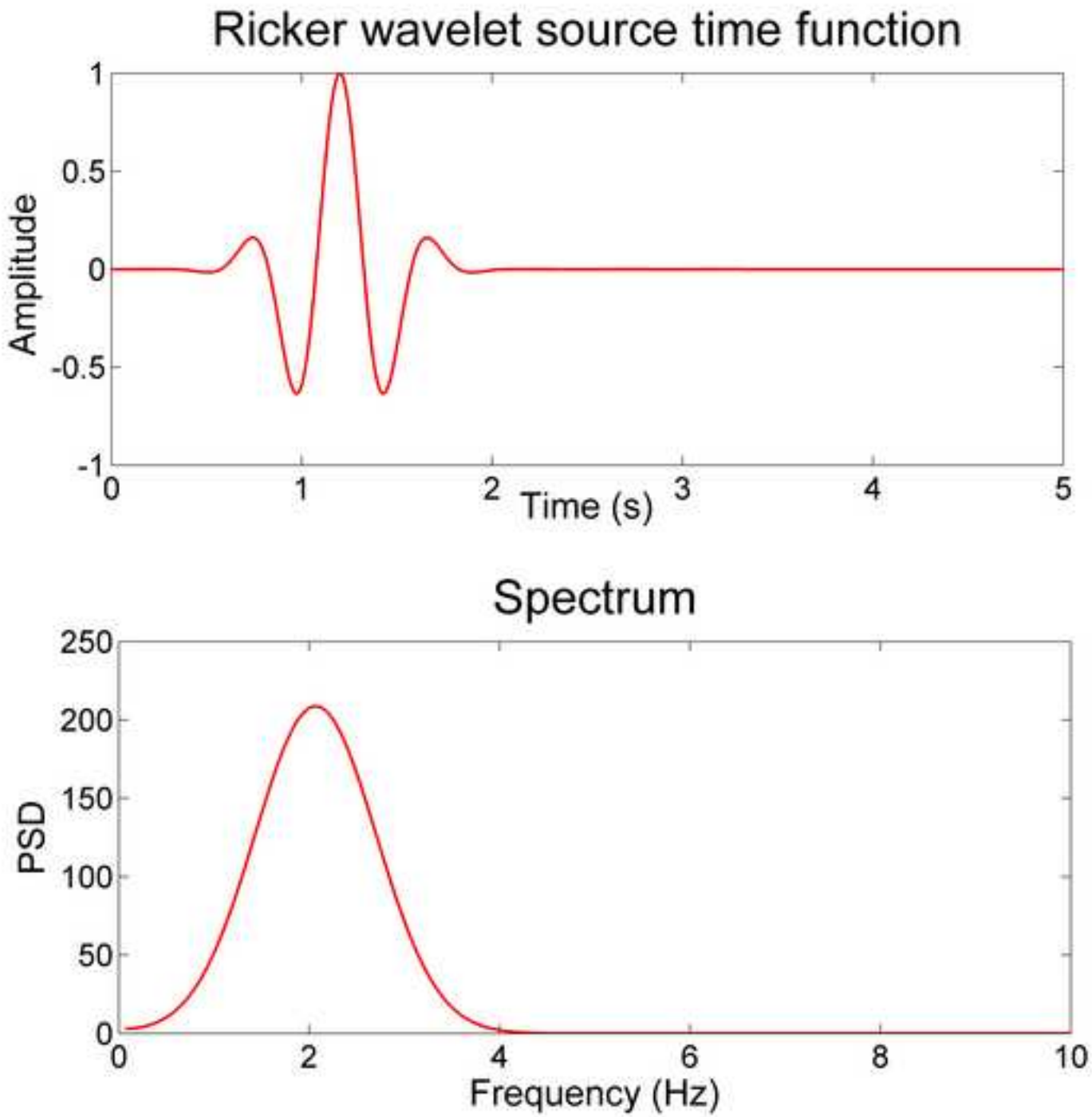

Figure 4

Click here to download high resolution image

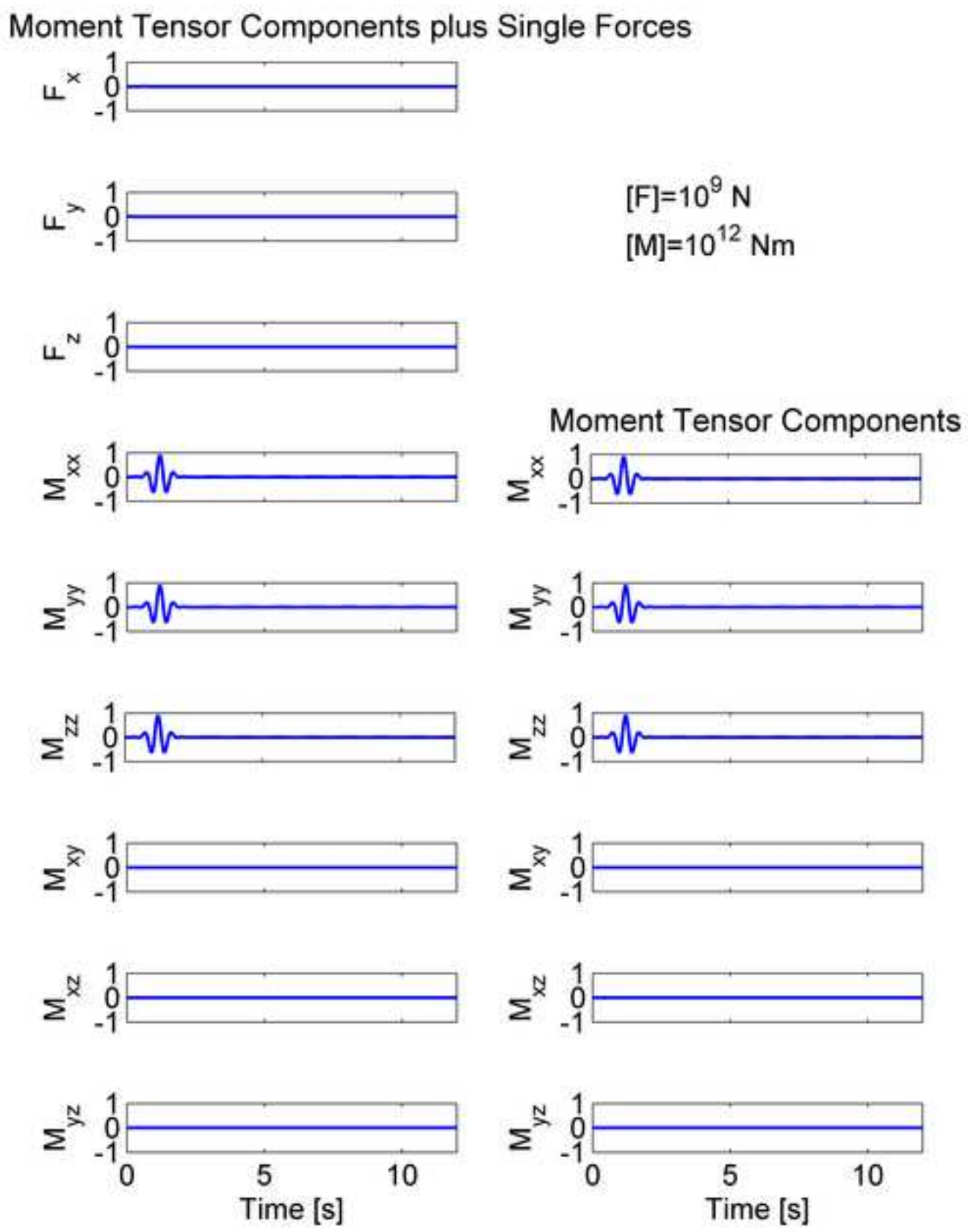

Figure 5

Click here to download high resolution image

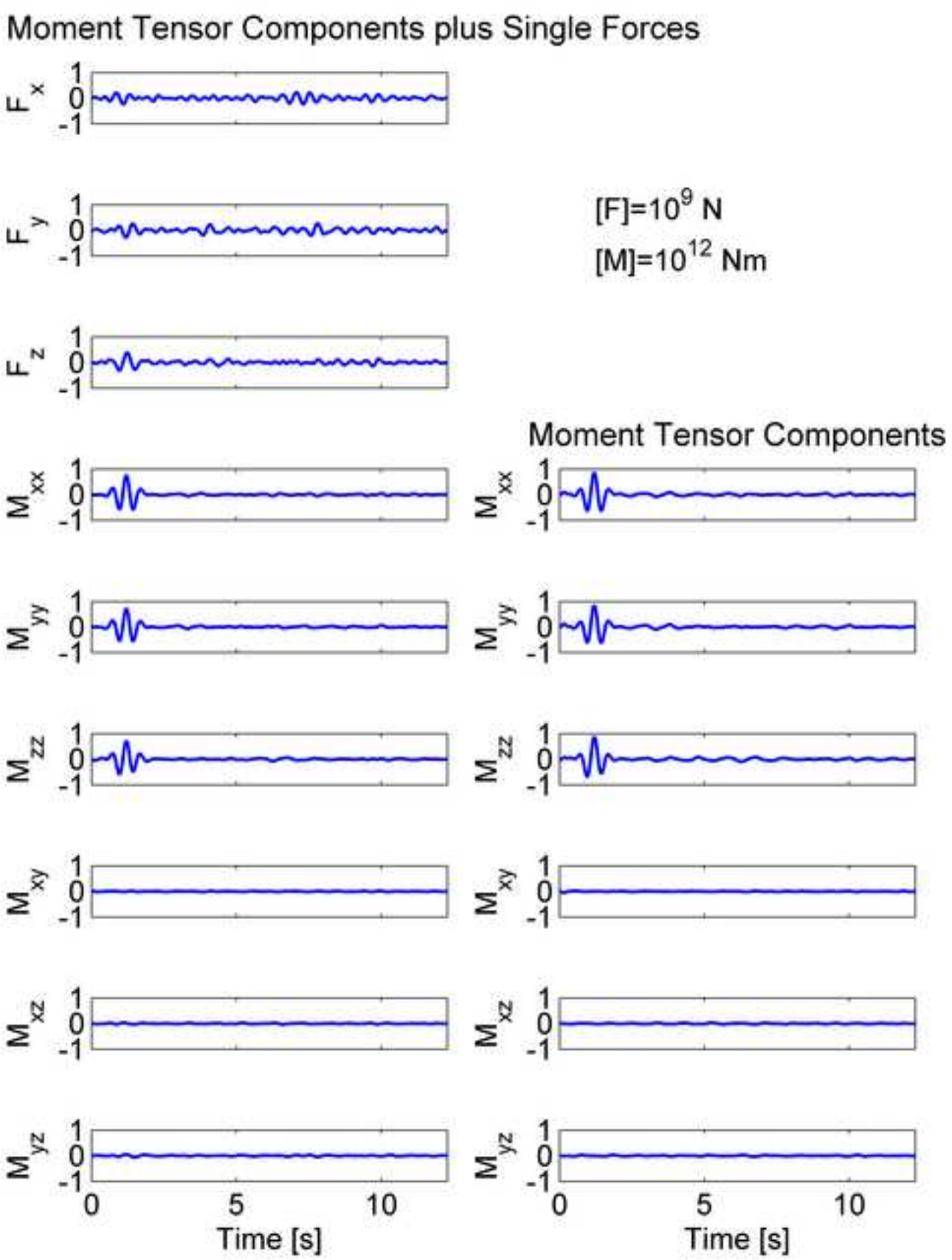

Figure 6

Click here to download high resolution image

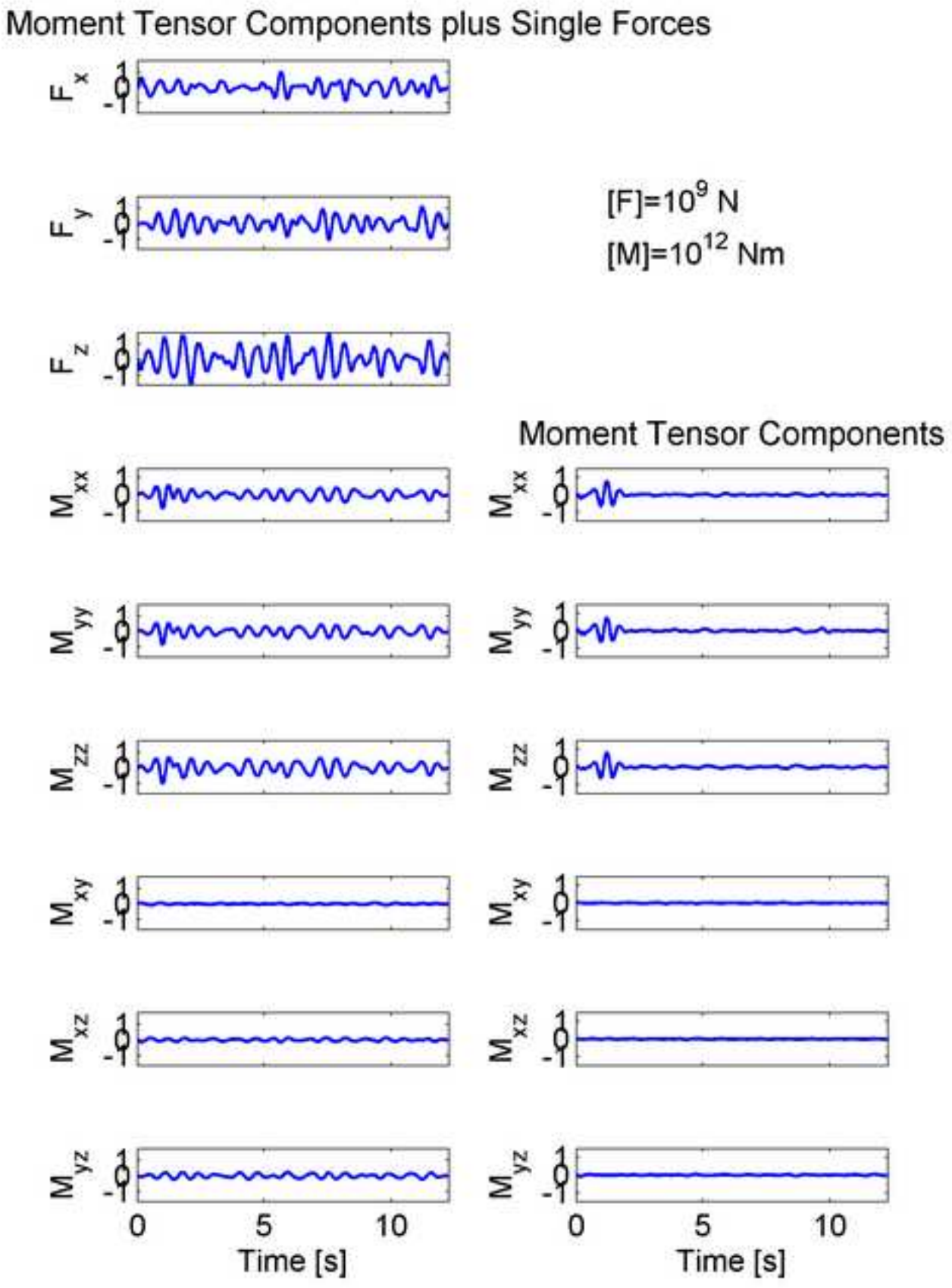

Figure 7

Click here to download high resolution image

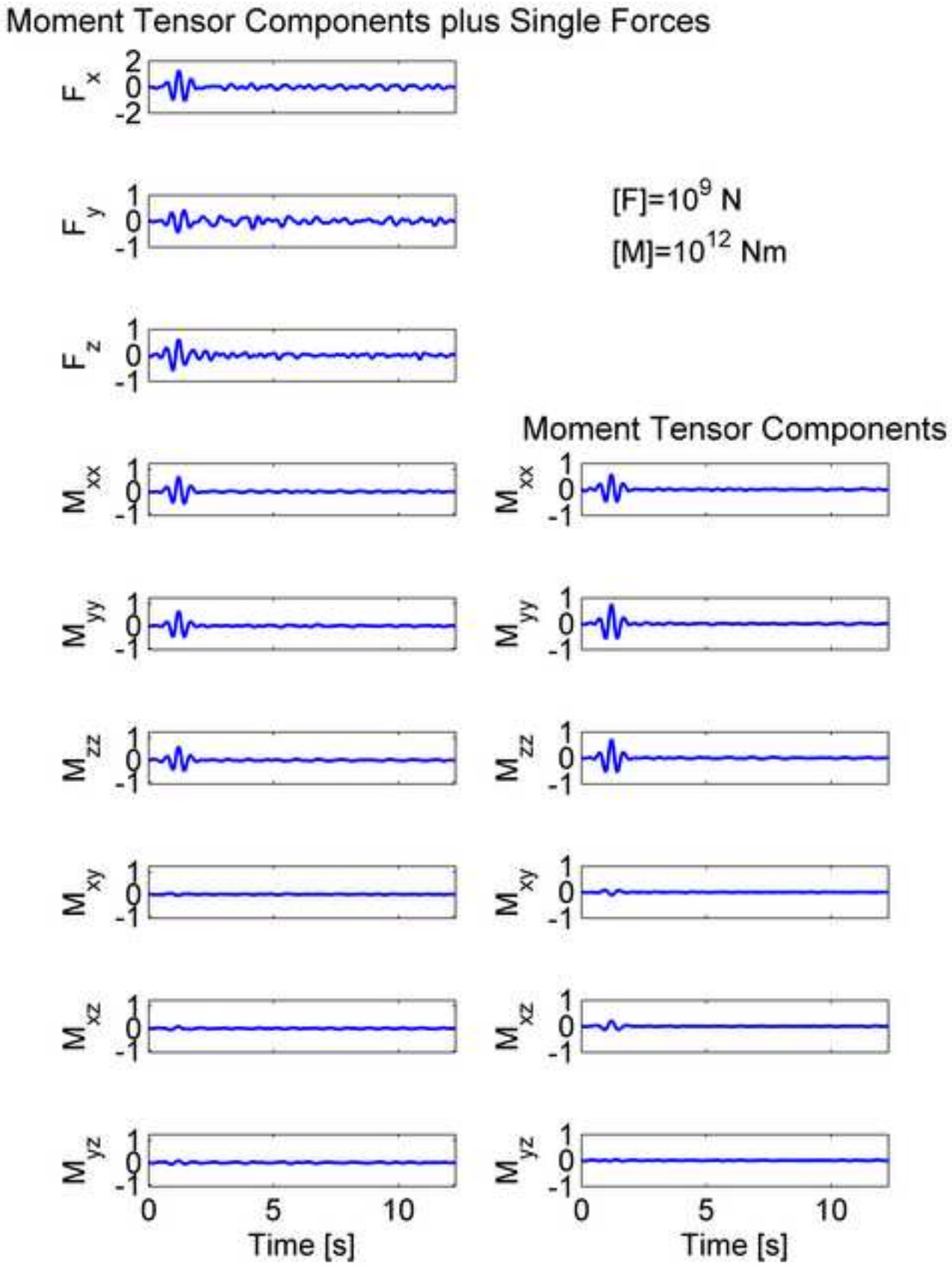

Figure 8

Click here to download high resolution image

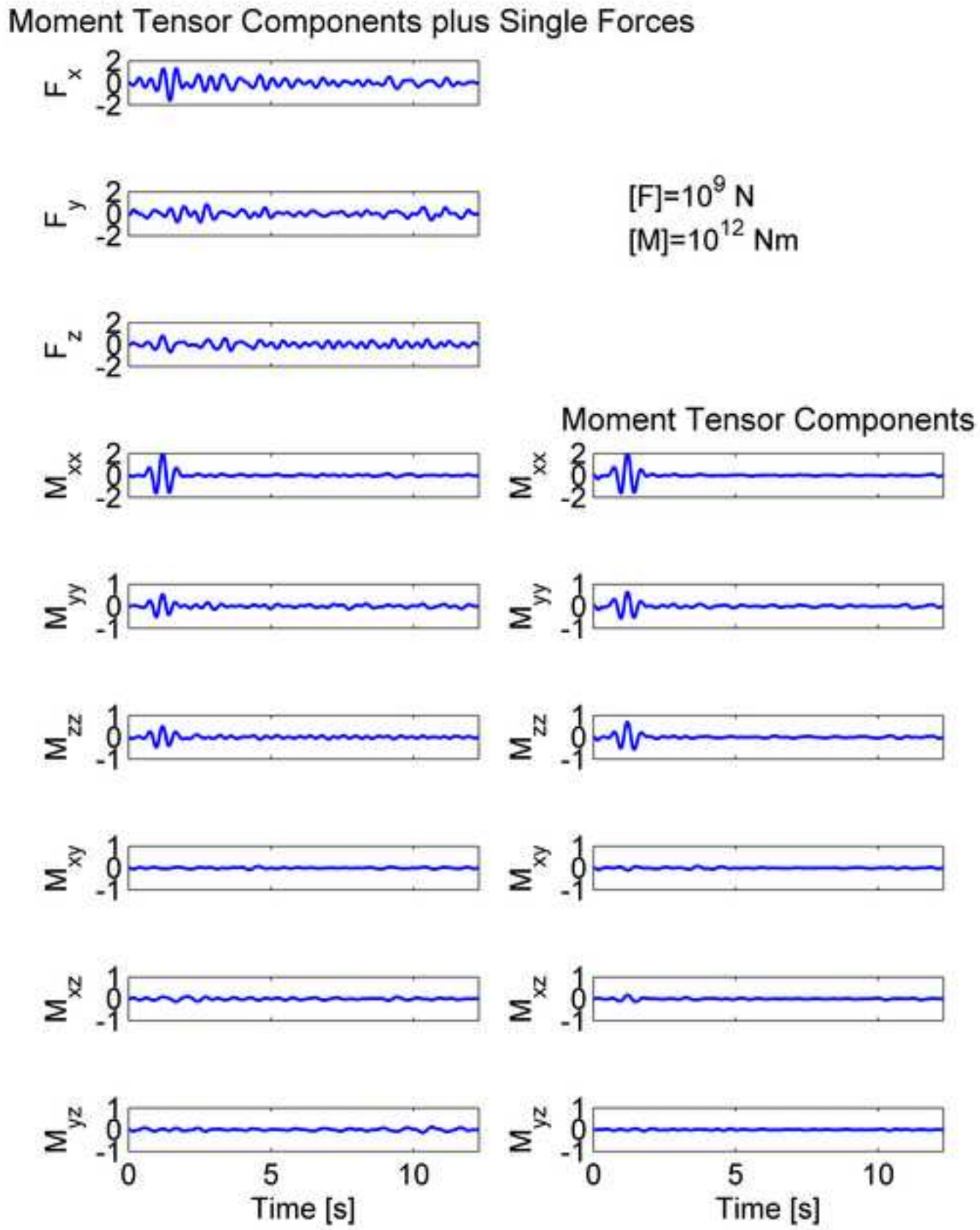

Figure 9

Click here to download high resolution image

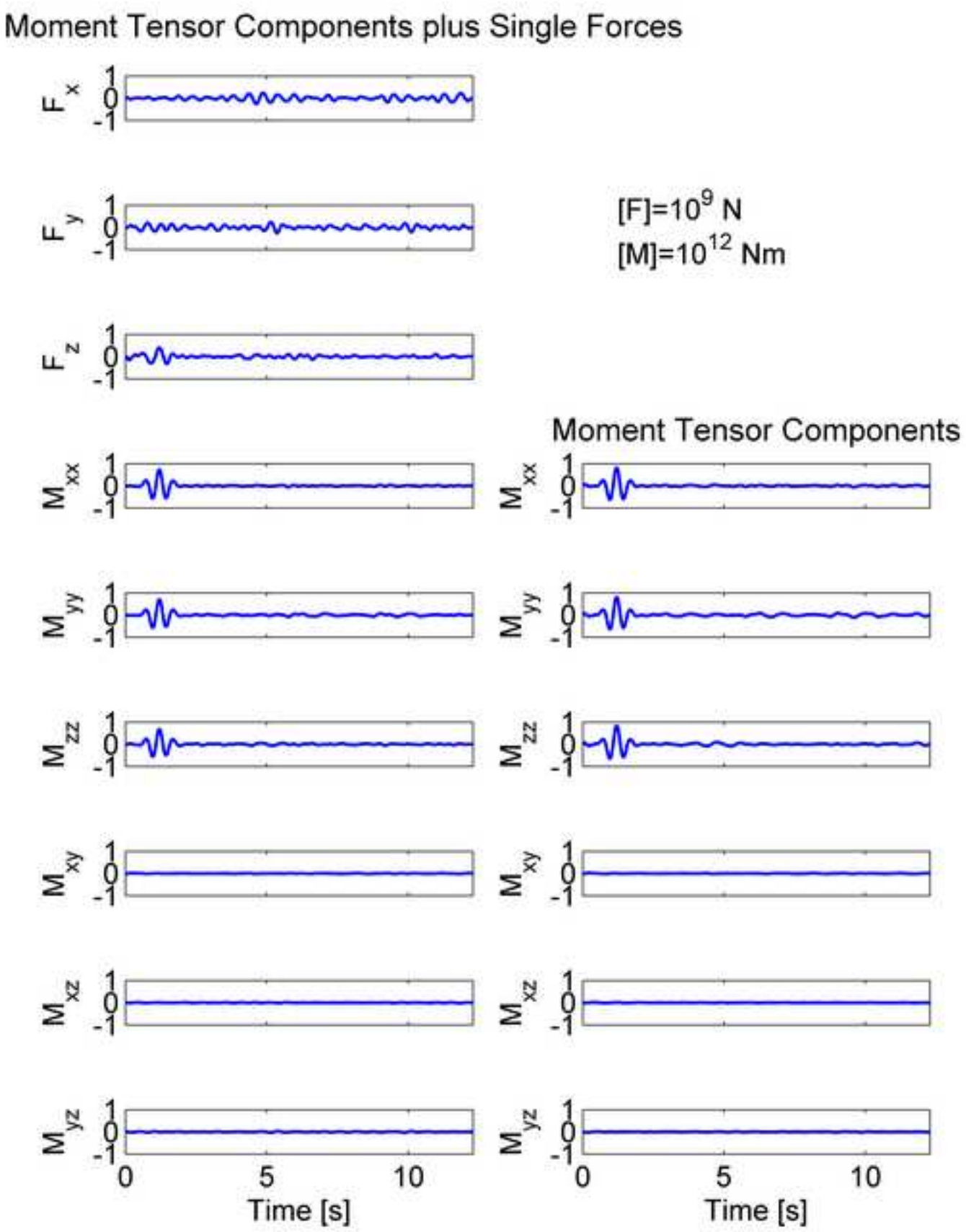

Figure 10

Click here to download high resolution image

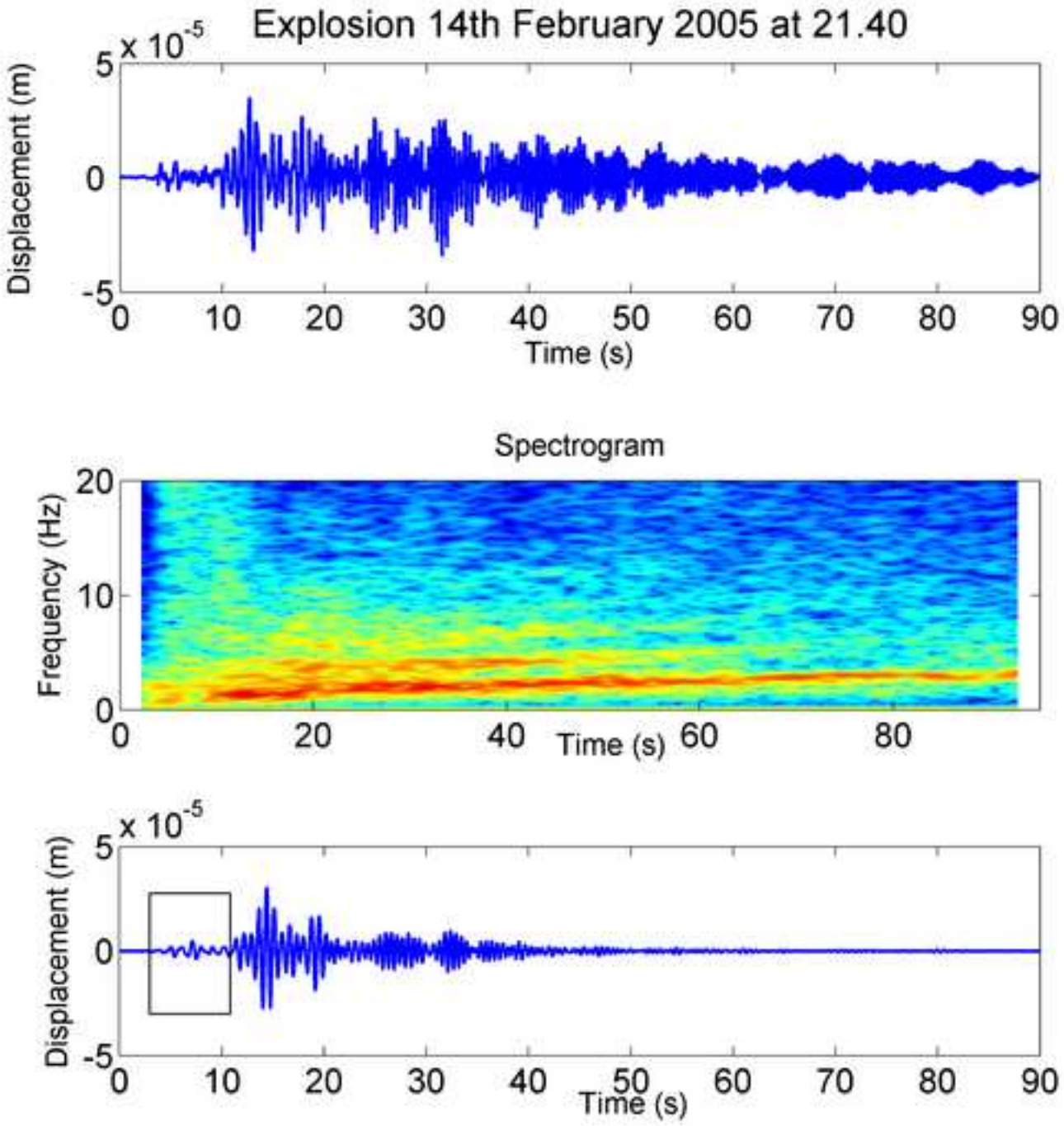

Figure 11

Click here to download high resolution image

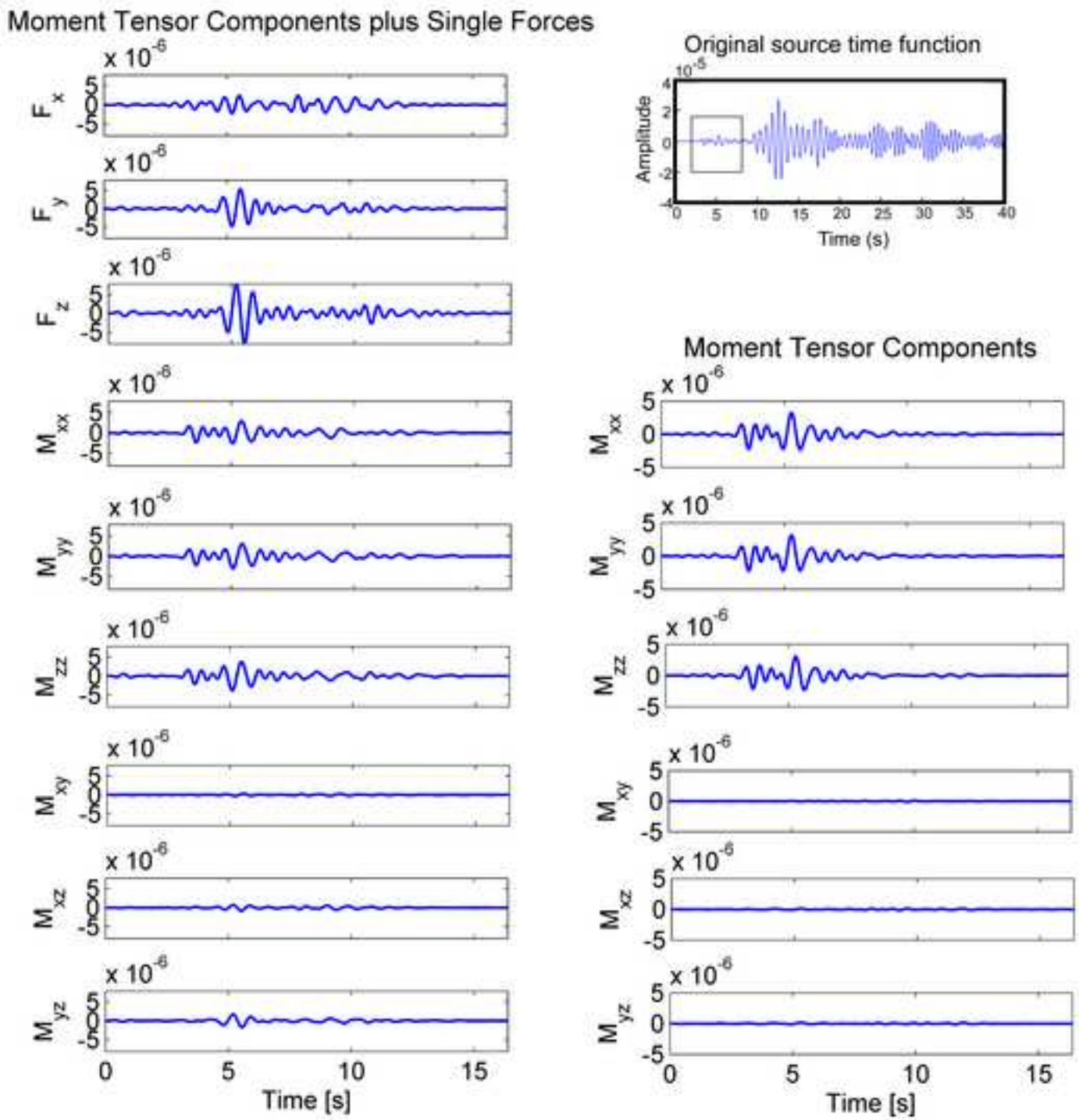

Figure 12

Click here to download high resolution image

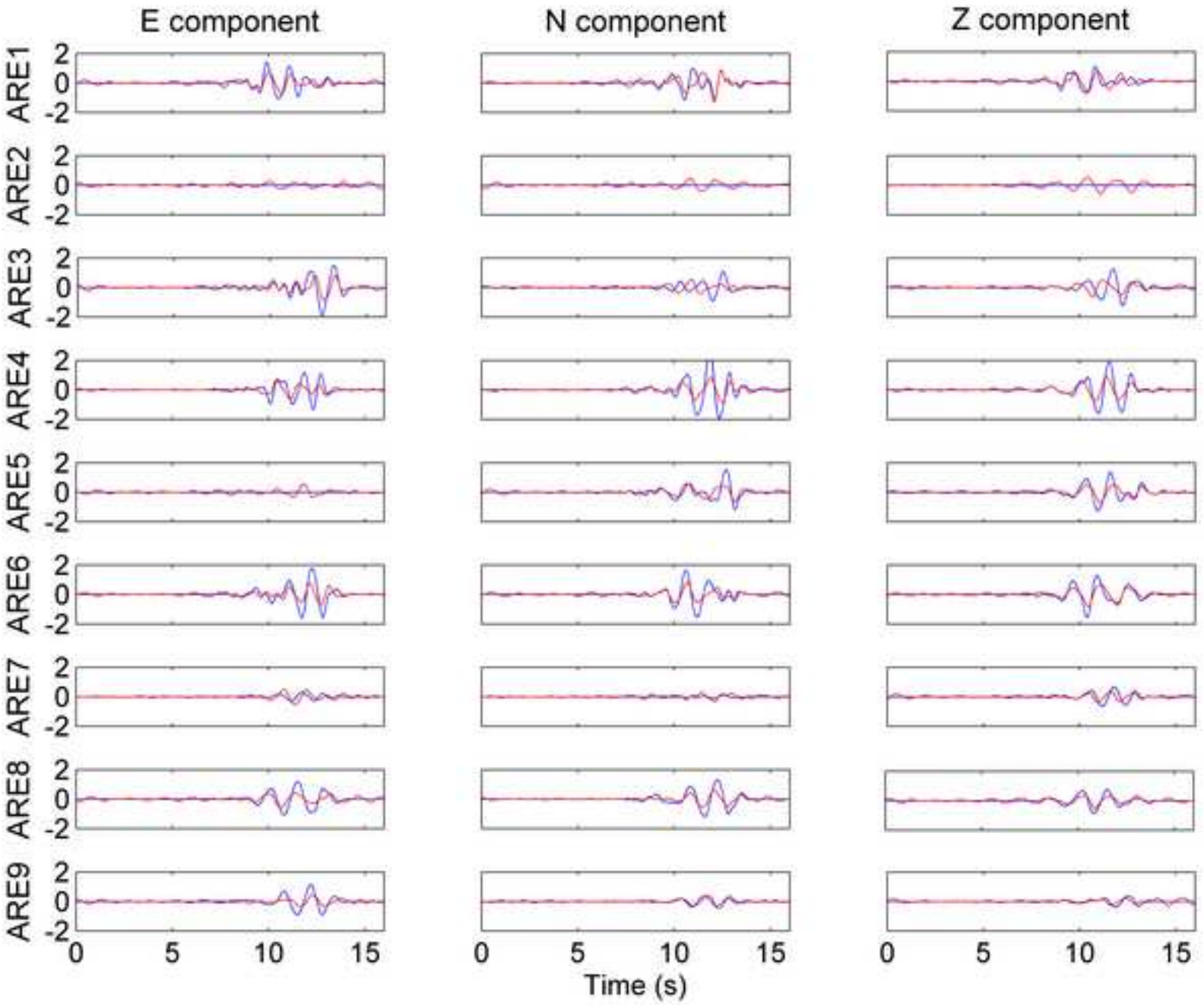

Figure 13

Click here to download high resolution image

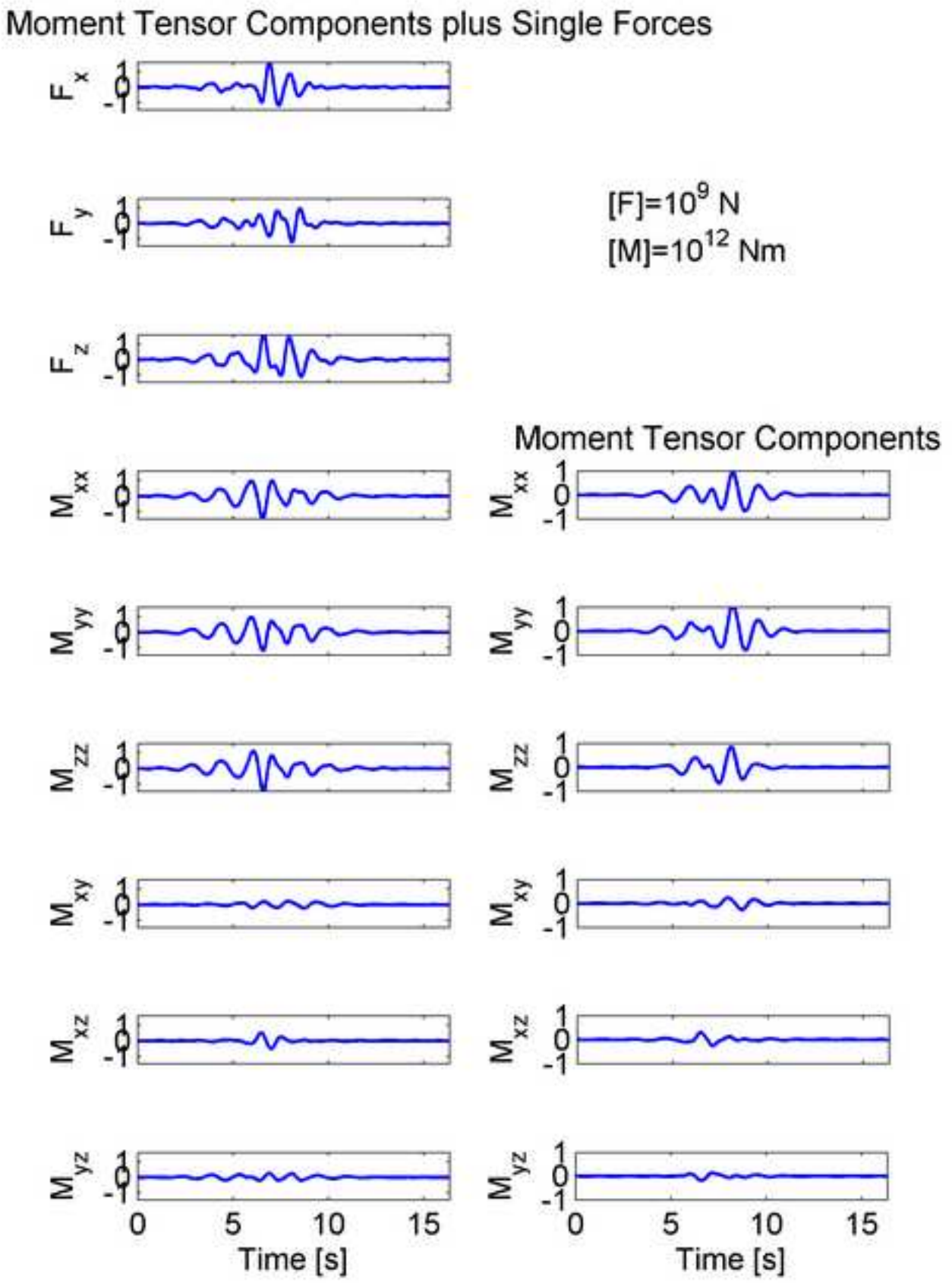

Table

Click here to download Table: Table 1.xls

Test n.	Description	S/N	Inverted components	Misfit (R)
1	data contaminated with random noise	10	MT	0.092
		10	MT + SF	0.086
2	data contaminated with random noise	2	MT	0.252
		2	MT + SF	0.226
3	data contaminated with random noise for a pure volumetric source geometry	10	MT	0.099
		10	MT + SF	0.083
4	data contaminated with random noise for a vertical crack source geometry	10	MT	0.103
		10	MT + SF	0.088
5	data contaminated with random noise for a mislocated source position	10	MT	0.097
		10	MT + SF	0.093
6	40 s long source time function		MT	0.092
			MT + SF	0.049
7	Explosion Feb 14th, 2005		MT	0.567
			MT + SF	0.418